

See discussions, stats, and author profiles for this publication at: <https://www.researchgate.net/publication/336730812>

Unscented Kalman Filter based Self-sensing Control of Shape Memory Alloy Actuator

Thesis · November 2017

DOI: 10.13140/RG.2.2.25892.22402

CITATIONS
0

READS
447

1 author:



Daiki Ikeuchi
University of Cambridge

16 PUBLICATIONS 86 CITATIONS

[SEE PROFILE](#)

Some of the authors of this publication are also working on these related projects:



CSIRO Cold Spray Additive Manufacturing [View project](#)



The University of Sydney
School of Aerospace, Mechanical and Mechatronic Engineering
HONOURS THESIS

UKF based self-sensing control of a shape memory
alloy actuator

Submitted in partial fulfillment of the requirements for the degree of
BACHELOR OF ENGINEERING HONOURS (MECHANICAL)

by

Daiki Ikeuchi

November 2, 2017

Acknowledgements

First and foremost, I would like to express my gratitude to my supervisor, Dr. Xiaofeng Wu, for his consistent support, encouragement and consideration throughout the duration of this Honours thesis.

Secondly, I would like to appreciate the supports from my friends and peers at the University of Sydney, who have given sincere advices on academic writing, MATLAB programming and general engineering issues. Also, their times and efforts in proofreading this thesis are greatly appreciated.

Finally, I would like to thank my parents, who have given me an opportunity to study overseas and supported me both financially and mentally throughout the year.

Preface

This Honours thesis is presented for those with general engineering background, but without familiarity with the topic of this thesis. Although it is not necessary to possess the thorough understanding of a shape memory alloy, materials science and control principles of nonlinear systems, some familiarities are recommended to appreciate the scope of the thesis.

All works presented in this thesis were carried out and completed in a partial fulfillment of the requirements for the degrees of Bachelor of Engineering Honours (Mechanical) in the School of Aeronautical, Mechanical and Mechatronic Engineering at the University of Sydney between March 2017 and November 2017.

While a substantial portion of this thesis is of my own works, some of the models and ideas have originated from the works of others in the literature. In such cases, a proper referencing is used to differentiate others from my own as listed below.

- I conducted the literature review on basic shape memory alloy actuators and their control strategies to propose the topic of this thesis.
- I designed numerical models for a spring-biased SMA wire actuator.
- I designed numerical models for Unscented Kalman filters.
- I performed and analyzed all simulations in MATLAB and Simulink.

DAIKI IKEUCHI

SUPERVISOR, DR. XIAOFENG WU

Abstract

The numerical feasibility of a Dual Unscented Kalman Filtering algorithm has been investigated in terms of estimation accuracy. Combined with the estimation algorithms, the self-sensing property of a shape memory alloy is utilized to obtain the electrical resistance measurements through the nonlinear SMA models. These are all integrated into a closed-loop feedback system with a simple PID controller to actively control the displacement of the SMA actuator to study the tracking accuracy.

The results show reasonably accurate estimations in both state and parameter filters, based on which the actuated displacement is estimated. Two different displacement profiles have been tested with both results showing an acceptable agreement with the reference displacement profiles.

The results of this study suggests that it is numerically feasible to use the Dual Unscented Kalman Filtering algorithm for a better tracking control in the context of a shape memory alloy actuator.

Contents

List of Figures	xi
List of Tables	xiii
1 Introduction	1
1.1 Shape memory alloy actuators	1
1.2 Control of a shape memory alloy actuator	2
1.3 Research question	3
1.4 Significance of the study	3
1.5 Outline of the Study	4
2 Relevant Concepts	5
2.1 Shape Memory Alloy (SMA)	5
2.2 Shape memory alloy actuator	6
2.2.1 Bias type SMA actuator	7
2.2.2 Antagonistic type SMA actuator	7
2.3 Nonlinearity and Hysteresis	8
2.4 Uncertainties	10
2.5 Kalman filtering	10
3 Literature Review	13
3.1 Smart materials actuator	13
3.1.1 Piezoelectric actuator	13
3.1.2 Copper and Iron-based shape memory alloy	15
3.2 Control of a nonlinear dynamics SMA actuator	16
3.2.1 Sliding Mode Control	16
3.2.2 Adaptive Control	19

3.3	State estimation	21
3.3.1	Kalman Filter	22
3.3.2	Extended Kalman Filter	22
3.3.3	Unscented Kalman Filter	24
3.4	Self sensing control	25
4	Modeling of a shape memory alloy actuator	27
4.1	Spring biased SMA wire actuator	27
4.2	Shape memory alloy modelings	29
4.2.1	Heat transfer model	30
4.2.2	Phase transformation model	30
4.2.3	Constitutive model	32
4.2.4	Kinematic and actuator dynamic model	32
4.2.5	Electrical resistance model	33
4.2.6	Summary of SMA model and materials parameters	34
4.3	Dual Unscented Kalman Filter algorithms	34
4.3.1	Unscented Transformation	36
4.3.2	State UKF estimation algorithm	36
4.3.3	Parameter UKF estimation algorithm	40
4.4	Closed loop control	43
4.4.1	PID controller design	44
5	Results	47
5.1	SMA model validation	47
5.2	State UKF performance analysis	47
5.2.1	Single square wave	49
5.2.2	Sinusoidal wave	49
5.3	Realistic noise analysis	52
5.4	Robustness to external disturbance	52
5.5	Parameter UKF performance analysis	55
5.6	Tracking performance analysis in closed-loop control	57
5.6.1	Tracking performance with State UKF	57
5.6.2	Tracking performance with DUKF	59
6	Discussion	61

6.1	State UKF estimation	61
6.2	Parameter UKF estimation	62
6.3	Actuator tracking performance	63
7	Conclusion	65
7.1	Future Work	66
	Bibliography	69

List of Figures

2.1	SMA phase transformation overview	7
2.2	Rotary bias type SMA actuator	8
2.3	Nickel-Titanium (NiTi) SMA phase transformation	9
3.1	Control algorithms for SMA actuators	17
3.2	Sliding model stress based control	18
3.3	Variable Structure Control	18
3.4	Schematic of a Neural Network Structure	19
3.5	Schematic of Forward Neural Network training	20
3.6	Fuzzy logic gain adapted PID control	20
3.7	Schematic of Extended Kalman Filter	23
3.8	Transformation temperature dependency on stress	24
3.9	UKF and EKF performance comparison	25
3.10	Hysteresis between electric resistance and strain	26
4.1	Working mechanism of a SMA wire actuator	28
4.2	Schematic diagram of SMA wire actuator	29
4.3	Schematic diagram of Dual Unscented Kalman Filter algorithm	42
4.4	Overview of the UKF based closed-loop control block diagram	43
4.5	An example of practical electrical resistance measurement methods	44
4.6	A schematic diagram of PID controller	45
5.1	Model validation - temperature vs strain	48
5.2	State UKF estimation to single square voltage wave	50
5.3	State UKF estimation to sinusoidal wave	51
5.4	Approximate temperature external disturbance profile	52
5.5	State UKF estimation under noisier condition	53

5.6	State UKF estimation with external disturbance	54
5.7	Empirical convective heat transfer coefficient UKF estimation	55
5.8	Thermal expansion factor UKF estimation	56
5.9	Displacement tracking performance in stair-case wave	58
5.10	Displacement tracking performance in sinusoidal wave	58
5.11	Comparison between UKF and DUKF	60
6.1	Control voltage input to stair wave displacement profile	63

List of Tables

3.1	NiTi SMA and Piezoelectric actuator performance comparison	14
4.1	Model and nominal materials properties	34
4.2	UKF filter parameters	43
4.3	PID controller gains	45

List of Acronyms

DSC Differential Scanning Calorimetry.

DUKF Dual Unscented Kalman Filter.

EKF Extended Kalman Filter.

FLC Fuzzy Logic Control.

GRV Gaussian Random Variable.

KF Kalman Filter.

LTI Linear Time Invariant.

NiT_i Nickel-Titanium.

NNC Neural Network Control.

PE Pseudoelasticity.

PEA Piezoelectric actuator.

PID Proportional-Integral-Derivative.

PWM Pulse Width Modulation.

PZT lead zirconate titanate.

SMA Shape Memory Alloy.

SMC Sliding Mode Control.

SME Shape Memory Effect.

UKF Unscented Kalman Filter.

UT Unscented Transformation.

VSC Variable Structure Control.

List of Nomenclatures

A_f Austenite finish temperature.

A_s Austenite start temperature.

M_d Martensite dead temperature.

M_f Martensite finish temperature.

M_s Martensite start temperature.

While there had been a wide range of actuator types available, including hydraulic, pneumatic, electric and mechanical, it was not until mid 1980s that the electroactive functional materials started attracting research attentions in an attempt to integrate them into mechanical structures such as actuators and sensors [1], introducing a concept of smart materials actuators. These smart materials-based actuators offer actuating and sensing abilities in a controlled manner by external stimuli (e.g. stress and temperature). The subject of smart material-based actuators has increasingly been of great research interests due to their superior properties such as compactness, simplicity, maintainability and silence operation [2].

1.1 Shape memory alloy actuators

Following the research popularity in smart materials actuators, a number of key smart materials has been extensively studied and utilized in the development of mechanical structural systems, including Shape Memory Alloy (SMA), Piezoelectric and Magnetostrictive materials. Among these materials, a shape memory alloy is most widely used as an actuator material in a variety of engineering industries such as biomedical, automotive, aerospace and robotics [3]. Since its first discovery in the early 1930s [4], the alloy was not given much research attentions until Buehler et al. [5] brought the Shape Memory Effect (SME) to light in a Nickel-Titanium (NiTi) alloy, presently

known as nitinol. The SME is best described as the ability of a shape memory alloy to retain a deformed shape after an external load is applied and removed, and then recover to its original memorised shape upon heating process [6]. With this unique property, a shape memory alloy offers great ductility, excellent corrosion resistance, stable transformation temperatures, compactness and high force to weight ratio [7], [8]. Due to these advantages over other smart materials, a NiTi-based SMA gains much attentions in actuator applications where reduced weight, large displacement, compact size and noiseless operation are strongly demanded. This indicates a high potential of such actuators as an alternative to the conventional actuators.

1.2 Control of a shape memory alloy actuator

Although the shape memory alloy based actuators exhibit many physical advantageous behaviours and they have been researched in the last few decades, the use of shape memory alloy as an actuator still remains uncommon compared with conventional actuators, especially as an active actuator. One of the main reasons for this trend is associated with the control difficulty of these actuators, resulting mainly from nonlinearity, hysteresis and uncertainties. Nonlinearities arise from the complex temperature dependent stress-strain relationship in the SMA actuating mechanism [9]. Hysteresis effects are observed in the relationships between displacement and temperature, modulus of elasticity and temperature, displacement and voltage, strain and temperature, and martensitic fraction (fraction of phase in martensitic state of SMA) and temperature [9]. Another control difficulty, uncertainties, is due to the number of state variables (e.g. temperature and stress) and relevant internal parameters being extremely difficult or impractical to be measured accurately. The lack of knowledge of state variables poses a challenging task for the SMA control community on the implementation of model-based control algorithms because it requires the knowledge about state variables, including stress, temperature, martensitic phase fraction and kinematics of the actuator system [10]. For miniature applications where SMA actuators are highly demanded, it is often not desirable to integrate physical sensors into the system, which further limits the state variable information available for model-based control algorithms. Parameter uncertainties amplify the deviation between the actual physical system and utilized models, leading to an inaccurate control of the SMA actuator. For

the successful applications of a shape memory alloy-based actuator in high-precision control areas, it is essential to overcome the aforementioned aspects of control difficulty.

1.3 Research question

Despite the great amount of research in the fields of model-based control algorithms to tackle nonlinearity and hysteresis problems, there has not been much research focus on the development of a control strategy to improve the issues associated with the lack of state variable information due to measurement difficulties, and parameter uncertainties. This gives a motivation to the author to design a model-based estimation and control algorithm for solving these control difficulties of the SMA actuator for more accurate and practical applications. Given the inspiration from simultaneous state and parameter estimations for autonomous vehicle control using Extended Kalman Filter (EKF) in [11], in this study, the author proposes to design a dual Unscented Kalman Filter (UKF) model-based state and parameter estimator for a simple spring-biased SMA wire actuator and investigate the numerical feasibility of the estimation algorithms. To overcome the lack of availability of measured state variables, the self-sensing property of a shape memory alloy is to be also studied to integrate into the UKF based closed loop controller to mitigate the needs of physical sensors on the actuator.

1.4 Significance of the study

Many model-based control algorithms often assume the complete knowledge of all state variables or at least the states variables of interest, which are not always available or impractical to measure due to the lack of sensors for miniature applications where SMA actuators are utilized. Through this study, the numerical feasibility of dual UKF technique in the context of a shape memory alloy wire actuator is to be studied and its performance is to be investigated from the perspective of estimation and control accuracies by comparing against the state variables and parameters collected through model simulations in imitation of the numerical feasibility study of Extended Kalman Filter (EKF) state estimation for a SMA actuator [12]. To the best of the

author's knowledge, these works have never been carried out by any others using Dual Unscented Kalman Filter configuration in the context of shape memory alloy actuators. The findings of this study are expected to contribute to the SMA actuator control community to raise the awareness of significance of mitigating state and parameter uncertainties in terms of high-precision control through the use of UKF estimation algorithms. Additionally, in combination with UKF estimations, the implementation of a self-sensing technique should allow the development of a closed loop control system, which does not require any physical sensors in practice. This has a high potential to be integrated into any systems where weight and space minimization is one of the main priorities.

1.5 Outline of the Study

In this thesis, Chapter 2 presents an overview of the relevant concepts for shape memory alloy actuator, its control difficulties and model-based control. Chapter 3 presents a review of the literature in the fields of SMA materials, its actuator applications, model and non model-based control algorithms, and self-sensing property of shape memory alloys and its applications. Chapter 4 outlines the modeling of nonlinear dynamics of a NiTi shape memory alloy based wire actuator, self-sensing, UKF estimation algorithms and the closed-loop control model with a simple PID controller. The results are presented in Chapter 5, followed by discussion of the performance of the estimation and control algorithm in Chapter 6. Chapter 7 presents the insights into potential extension to this study, as well as the conclusion based on the results and discussions.

2.1 Shape Memory Alloy (SMA)

Shape memory alloys are a class of metallic alloys, which are distinguished from conventional metallic alloys by their ability to retain a deformed shape after an applied external stimulus is removed and return to their original form (shape or size), when subjected to a memorization process, upon heating treatment, significantly exceeding the elastic deformability of the material. This ability is commonly termed as a Shape Memory Effect (SME) characteristic. This unique behavior of these alloys is attributed to the so-called martensitic phase transformation in the solid state [13].

Shape memory alloys possess two different phases in their solid state, namely high temperature austenitic phase and low temperature martensitic phase, in three different crystal structures (i.e. twinned martensite, detwinned martensite and austenite) and six possible crystallographic transformations [14]. At room temperature, a shape memory alloy is stable in its twinned martensitic structure, which transforms into the detwinned martensitic structure, resulting in a large deformation under a loading condition. Upon heating, a shape memory alloy starts to change its phase from martensite to austenite by diffusionless shear lattice distortion at austenite start temperature, A_s , and this transformation finishes at austenite finish temperature, A_f . In this case, the word diffusionless means that NiTi atoms remain at their lattice positions, but only the crystal orientation changes from non-cubic B19' structure to

2. RELEVANT CONCEPTS

ordered cubic B2 structure. Once the SMA temperature exceeds beyond A_f , it reverts to its original memorized form and this phenomenon can occur even under high applied loads, leading to high actuation energy density [15]. The highest temperature that this phenomenon can be observed is termed martensite dead temperature, M_d , beyond which a SMA deforms like other ordinary metallic alloys. Upon cooling process, a SMA starts to transform back into its martensite state at martensite start temperature, M_s and completes at martensite finish temperature, M_f as shown in Figure 2.1. These cyclic phase transformations take place at characteristic transformation temperatures (i.e. M_s , M_f , A_s and A_f), which may change over time due to thermal and stress cyclings [16]. The measurement of transformation temperatures is conducted using a Differential Scanning Calorimetry (DSC) test on ASTM standard [13].

The phase transformation in such a heating-cooling cycle is termed as one way SME and is commonly utilized in commercial applications. By having a shape memory alloy memorized its shape at both high and low temperatures, a two way SME can be achieved, resulting in a reversible shape change. However, due to the training requirements and its capability of producing only half the recovery strain of one way SME, the two way effect is often not utilized in shape memory alloy applications, especially in actuators. Another important characteristic of a shape memory alloy is Pseudoelasticity (PE), which allows it to retain the memorized shape under external stimuli between A_f and M_d .

2.2 Shape memory alloy actuator

A shape memory alloy actuator is designed based on the requirements of mechanical actuation (e.g. linear or angular displacements) and the corresponding force or torque. With the commonly utilized one-way SME as discussed in Chapter 2.1, the SMA-based actuators can only provide one-way actuation, which motivates the use of some mechanical bias mechanism to revert the SMA back to its detwinned martensite state for repetitive actuation [13].

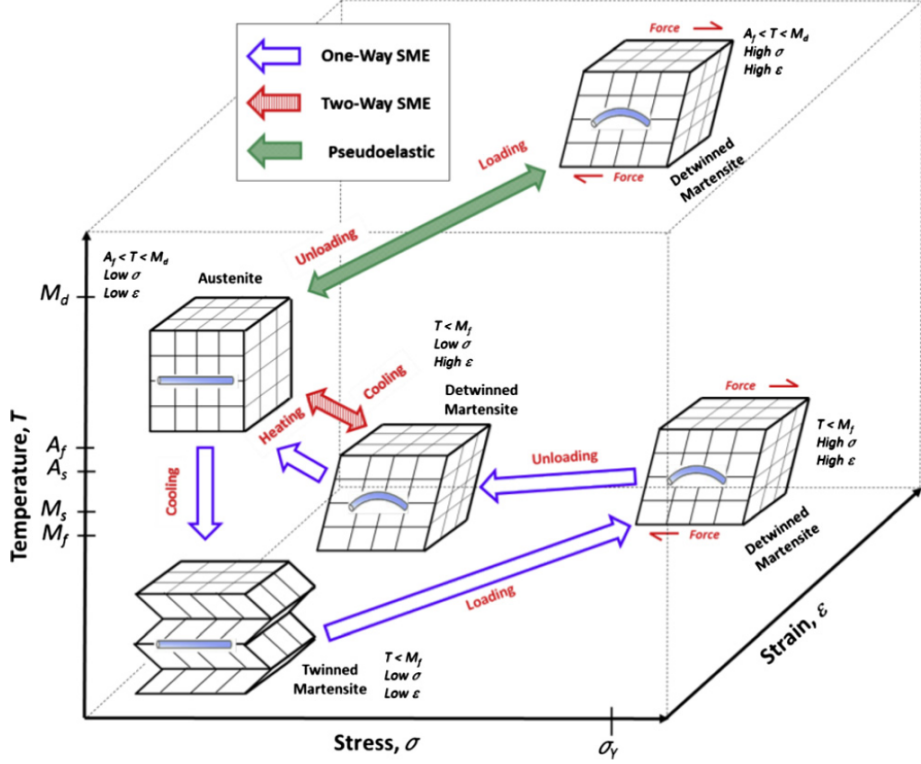


FIGURE 2.1: SMA phase transformation overview [3]

2.2.1 Bias type SMA actuator

One of the most common types of a SMA actuator bias mechanism is the use of constant load (e.g. weight) or a bias spring as shown in the one-way rotary SMA actuator in Figure 2.2. This mechanism is quite simple to fabricate with simple mathematical model, while it is more challenging in control perspective due to its one directional actuation [17]. In general, shape memory components in this bias configuration are in simple tension. Upon cooling process, the SMA element places itself back to its original position as the bias force from the spring overcomes the force applied by a SMA actuator.

2.2.2 Antagonistic type SMA actuator

An alternative configuration to provide the restoring mechanism of a shape memory alloy actuator is of antagonistic type where multiple SMA elements are implemented to provide restoring force to each other. This type of the SMA actuator offers a number of advantages over the bias type actuator such as higher degrees of motion control, the

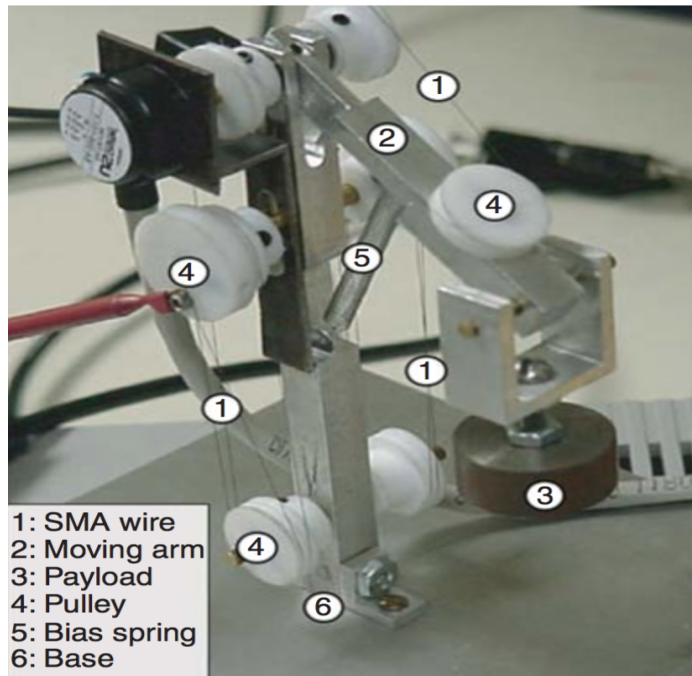


FIGURE 2.2: Rotary bias type SMA actuator [17], [18]

increased bandwidth, and higher efficiency of actuation [13]. Yet, control difficulties are more pronounced in this actuation configuration, preventing from the prevalence in practical actuator applications with this mechanism.

2.3 Nonlinearity and Hysteresis

Nonlinearities and hysteresis of a shape memory alloy arise from the nature of its thermomechanical responses as it undergoes martensitic phase transformation [19]. A typical thermomechanical behavior of NiTi SMA under thermal cyclic load during the phase transformation is as shown in Figure 2.3 [20]. Figure 2.3 shows that upon cooling and heating, forward (austenite \Rightarrow martensite) and reverse (martensite \Rightarrow austenite) transformations are taken place respectively in different paths, resulting in a hysteresis gap (e.g. the half difference between A_f and M_s temperature for the average gap). Generally, it is rather defined between the temperatures at which a shape memory alloy is in 50% transformed to its austenitic phase during heating and in 50% transformed to martensitic phase during cooling. This hysteresis is the consequence of dissipation of energy due to the thermal variation under iso-stress conditions or the pseudoelastic re-

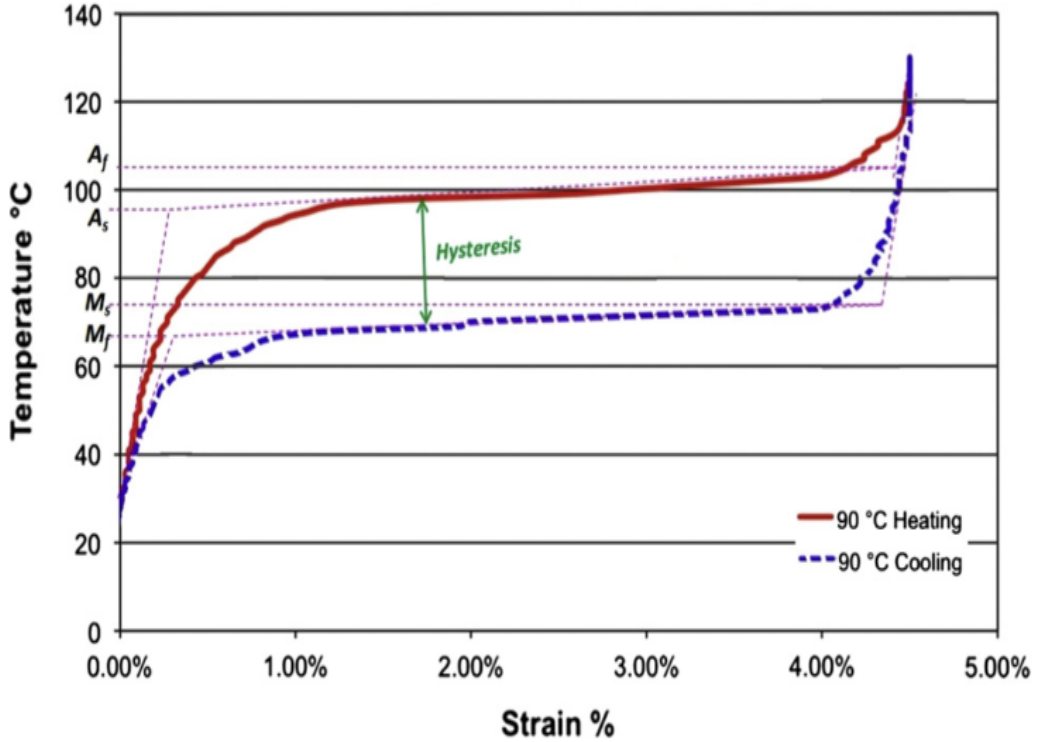


FIGURE 2.3: NiTi SMA phase transformation [20]

sponse [3]. During a number of initial thermal cycling of a SMA actuator, only a partial strain (or shape) recovery occurs upon heating with some irreversible permanent strain generated [13]. This residual permanent strain influences the stability of hysteresis behaviors, which is dominated by processing history, loading condition and the number of loading cycles [21]. The transformation paths also show severe nonlinearities between temperature and strain. A similar nonlinear hysteresis relationship can be observed between stress and strain, introducing a difficulty in the control of a SMA based actuator. This is because the complex nonlinear nature of a shape memory alloy is coupled with the co-dependent relationship between temperature, stress and martensite phase transformation. These nonlinearity and hysteresis loop behaviors are influenced by a number of factors, ranging from crystallographic properties (e.g. elemental composition and texture), manufacturing and post treatment process to fabricate into the actuator form (e.g. wire and spring) and operating conditions of a SMA actuator [22]. These factors further complicate the prediction of nonlinearities and hysteresis behavior during the operation of a SMA actuator, which deteriorates its precise control.

2.4 Uncertainties

There are mainly three categories of uncertainty associated with a shape memory alloy actuator system; that are state, model and parameter uncertainties. State uncertainties are the consequence of difficulties in the accurate measurement of internal state variables such as temperature and stress. For example, the temperature of a SMA actuating device is most likely not distributed uniformly if heated via Joules heating method (i.e. heated by passing an electrical current) [23]. Yet, it is often only possible to measure the temperature at the surface, resulting in uncertainties in internal temperature during phase transformation. A change in martensitic phase fraction of a SMA actuator is impossible to measure in practice during its operation, which is normally estimated using different phase transformation models during forward and reverse transformations [24] and [25]. Parameter and model uncertainties arise from a number of factors such as the model simplification, assumptions, circumstance-dependent and time-varying parameters. The models of a shape memory alloy behavior are divided into two main classes, micro-mechanical and phenomenological models [13]. Micromechanical-based model is formulated on microstructural information of a shape memory alloy to model the macroscopic response of a SMA actuating device, while phenomenological models utilize the principles of continuum thermodynamics to predict the simplified SMA responses. The former is more accurate and robust in terms of capturing macroscopic SMA responses, but due to more affordable complexity of models, most practical engineering SMA actuators are modeled phenomenologically (i.e. the latter modeling method), which introduces model uncertainties due to a number of underlying simplifications and assumptions. These models also utilize a number of nominal parameters measured at the macroscopic scale through experimental observations such as those from Liang et al. [24]. The nominal empirical parameters are often circumstance-dependent and time-varying (e.g. thermal expansion factor, phase transformation contribution factor and maximum residual strain [24]), which must be identified and updated for accurate control of SMA actuators.

2.5 Kalman filtering

The Unscented Kalman Filter (UKF) is a new variant of Kalman Filters (KF) proposed by Julier et al. [26] to introduce improvements to an Extended Kalman Filter (EKF)

in the control of nonlinear dynamics systems. Kalman filters are a class of recursive Bayesian filters, which utilizes a probabilistic method of using a prediction-correction cycle to estimate the state of a system from observed measurements and control inputs. It is one of the most commonly used state estimation methods in engineering applications due to its simplicity, tractability and robustness, but is only applicable to linear Gaussian systems to achieve the sufficient accuracy in estimations where the state transition and measurement probability are linear with the addition of Gaussian noise [27]. For almost any systems in practice, these conditions are not always satisfied. To apply the concept of Kalman filtering to nonlinear systems, the linear assumption of state transition and measurement probabilities are approximated by linearizing all nonlinear models using the first order Taylor series expansion so that the true posterior still holds Gaussian distribution with unimodal [27]. In EKF, there are still problems to control nonlinear systems; namely [26]

- Linearization may lead to unstable filters if the local linearity assumption is violated. In other words, the filter tends to be overconfident and causes an instability by rejecting any measurement information.
- The derivation of Jacobian matrices can be non-trivial in most practical applications, leading to a difficulty of implementation of the filter to the nonlinear dynamics system.

Julier et al. proposed to use a deterministic sampling approach to address these aforementioned issues in EKF [26]. With the specific and deterministic sampling algorithm using a set of carefully chosen sample points called sigma points, the posterior mean and covariance can be captured precisely to higher order of accuracy by passing the sigma points through an actual nonlinear dynamics system for any level of nonlinearity in comparison with EKF. Also, the need to calculate Jacobian matrices is eliminated through matrix operations, resulting in easier implementation of the filter [26]. Therefore, the UKF can provide more accurate estimation to the states of a nonlinear dynamics system such as the SMA actuator with less difficult implementation efforts.

3.1 Smart materials actuator

Smart materials have been increasingly attracting expectations in their unique characteristics to 'take a more innovative approach for making a high-performance actuator' [3]. Apart from a NiTi based shape memory alloy, there have been attempts to integrate other smart materials into the actuation mechanisms such as piezoelectric materials [28], [29]. To further study into the shape memory effects (SME) and pseudoelasticity, different alloy systems and their different elemental compositions have been investigated, mainly in iron and copper-based SMA systems [30], [31]. The basic knowledge of these alternative options is necessary to understand what the researchers have previously attempted and to support the selection of a NiTi based SMA actuator as a suitable candidate in this study with the expected high potential for practical applications.

3.1.1 Piezoelectric actuator

The use of a Piezoelectric actuator (PEA) is typically observed in micro/nano positioning applications in the fields of biomedical and robotics engineering due to its high hardness, fast response and other outstanding features [32]. These applications cover touch lithography, scanning probe microscopy, space flexible manipulators, and ultra-precision machine tools, to name a few [33], [34]. In general, the actuators are made

3. LITERATURE REVIEW

of piezoelectric ceramic materials, particularly lead zirconate titanate (PZT) being dominant ceramic to utilize [35]. The underlying concept behind these actuators is a fundamental process called piezoelectric effect, involving the linear electro-mechanical interactions and resulting in mechanical stress in its structural lattices when an electric field is applied [32]. This creates mechanical stress and strain, which cause actuation motion, yet on micro/nano scales. Therefore, by comparison with NiTi based SMA actuators, it has much lower work per volume as shown in Table 3.1.

Table 3.1: NiTi SMA and Piezoelectric actuator performance comparison adapted from [3]

Actuator type	NiTi SMA	Piezoelectric
Stress (MPa)	200	35
Strain (%)	8	0.2
Efficiency (%)	3	50
Bandwidth (Hz)	3	5000
Work per volume (J/cm^3)	10	0.035
Power per volume (W/cm^3)	30	170

Owing to these unique materials properties, a piezoelectric actuator possesses a number of outstanding advantages on nano scale such as a high precision positioning capability, high bandwidth (or fast response) and large output force. Main drawbacks, on the other hand, in its applications include nonlinearity, hysteresis and creep, which are similar to those of a shape memory alloy actuator [35]. The attempts to mitigate these control-related drawbacks are also taken similarly, effectively improving the capability of control of PEAs for nonlinearity and hysteresis, but there still exists problems associated with model and parameter uncertainties [36]. This suggests that the solutions to either a SMA or PEA could potentially be modified to solve the issue in another materials actuator. Overall, due to its greater actuation strain capability of 8% from Table 3.1, the SMA based actuators are expected to be utilized in a wider range of applications, compared with the PEAs where their main areas are of micro/nano fields. Therefore, the selection of a shape memory alloy actuator would be reasonable in this study to tackle control problems associated with uncertainties, while the solutions presented in this study may be applicable to the similar problems in piezoelectric actuator applications.

3.1.2 Copper and Iron-based shape memory alloy

Since the first discovery of the Au-Cd alloy showing the pseudoelasticity of a shape memory alloy [4], the shape memory effects and pseudoelasticity of the alloy have been observed in a large number of other alloy systems with different elemental compositions. Apart from the most common NiTi based shape memory alloy, copper-based alloys (e.g.Cu-Zn-Al and Cu-Al-Ni) [37] and iron-based alloys (e.g.Fe-Pt and Fe-Pd) [38] have been previously developed for specific applications in engineering.

A copper-based shape memory alloy was first given the attentions from researchers due to its affordability, simple fabrication and relatively good level properties [39]. Even though they do not have an excellent ductility ability, it is fairly easy to fabricate into components of almost any shape and size, which allows them to be studied without significant manufacturing and economical barriers. The initial simplest Cu-Al alloy was well defined for its shape memory characteristics with the main drawback of high characteristic transformation temperatures, which prevents itself from being utilized in commercial applications. This drawback was addressed by the inclusion of additional element such as zinc and nickel. The addition of a third element effectively reduced the grain size, which determines the overall properties of the shape memory alloy and produced the maximum recoverable strain of 5% in the Cu-Zn-Al system. The resulting Cu-Zn-Al and Cu-Al-Ni systems have been further studied and commercially become available on the market. The commercial uses of these alloys include civil pipe couplings and hydraulic fittings, mechanical dampers, and thermal actuator and sensor systems [40]. The remaining issues are the complex aging effects and relatively high transformation temperatures of these copper-based SMA.

The investigations of an iron-based shape memory alloy are relatively new compared with other shape memory alloy systems. Iron-based SMAs were studied and developed mainly in Japan in the basic Fe-Mn-Si alloy system in an attempt to develop an alternative to a NiTi and copper-based shape memory alloy for low cost [41]. Similar to the copper-based SMA development, additional minor elements were included into the system to improve shape memory alloy characteristics. These alloys are commonly utilized as joints due to their high recovery stress, rather than strain in other shape memory alloy systems, which make themselves suitable for large scale applications. However, the NiTi based SMA possesses more suitable shape memory characteristics than the ferrous SMA, and it is not recommended to replace NiTi with the iron-based

3. LITERATURE REVIEW

alloys in low to medium sized applications due to the relatively low benefits obtained from the use of a cheaper iron-based shape memory alloy [40].

In summary, the literature indicates that it is appropriate to select NiTi as a suitable material for actuator applications due to its higher recoverable strain and lower transformation temperatures than the copper-based SMA and superior shape memory characteristics than iron-based SMA in small scale applications.

3.2 Control of a nonlinear dynamics SMA actuator

Various attempts have been made by different researchers to investigate control algorithms for a nonlinear dynamics shape memory alloy systems in many engineering applications where accurate positioning is required as shown in Figure 3.1. In the early development of SMA actuator control strategies, Majima et al. [42] designed a conventional Proportional-Integral-Derivative (PID) feedback controller along with a Preisach model based feedforward loop to compensate for hysteresis effects. Modified PID feedback control algorithm was also presented by Shameli et al.[43], implementing an additional P^3 term and by Ma et al. [44] using a Pulse Width Modulation (PWM) based PD controller in an attempt to improve energy efficiency.

To further mitigate the hysteresis and its associated nonlinearities of a shape memory alloy actuator, the development of nonlinear control algorithms followed by many researchers including Sliding Mode Control (SMC) and Adaptive Control [9].

3.2.1 Sliding Mode Control

Sliding mode control is a class of nonlinear control algorithm that has favorable properties of accuracy, robustness and ease of implementation. This nonlinear control technique is especially demanded in an application where uncertainties are significant factors of operation, matching with the needs in SMA actuation. The basic concept of the algorithm is that the controller drives the states of a nonlinear dynamic system onto a 'sliding surface' in the state space where the system behaves like the reduced order system (e.g. Linear Time Invariant (LTI) system). When the state of a nonlinear system reaches near the sliding surface, the controller constrains the state close to

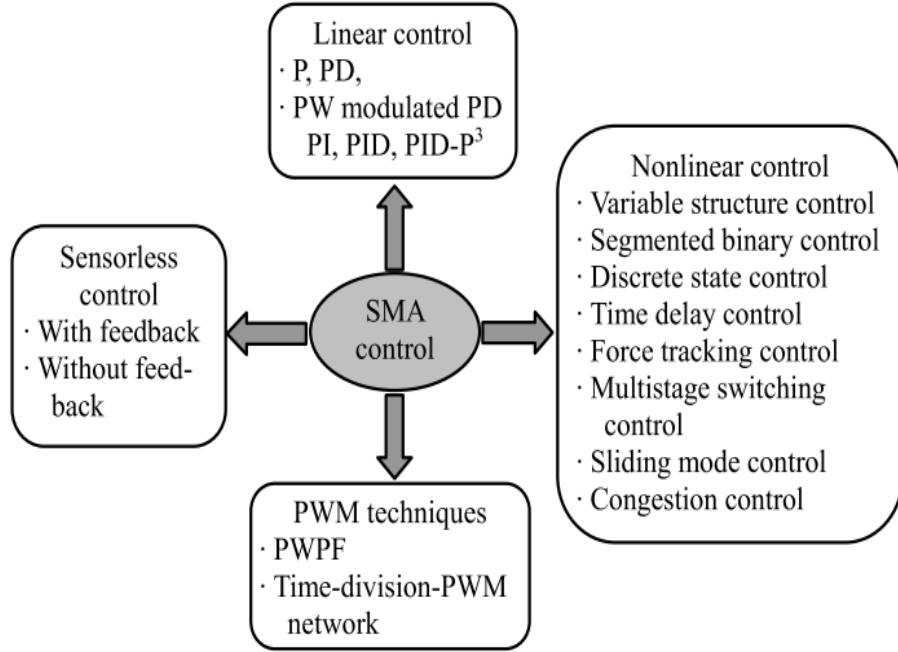


FIGURE 3.1: Control algorithms for SMA actuation [45]

the surface to govern the system by the dynamics of the reduced order system. Two important aspects of this nonlinear control are to [46]:

1. Design a sliding surface such that the sliding motion achieves the desired specifications of a nonlinear dynamics system (e.g. introduce a sliding mode variable $s = x_2 + \sigma x_1$ to approximate the 1st order system dynamics).
2. Select the control law such that a sliding surface exists and can be approached by the system.

The advantage of SMC in the context of a SMA actuator is that the closed loop response becomes less sensitive to uncertainties, including bounded parameter uncertainties and nonlinearities [46]. A number of researchers in the shape memory alloy control community have applied and integrated SMC into the NiTi based SMA actuator, ranging from Choi et al. to improve the response speed and tracking performance of SMA spring in a single link mechanism [47], to Lim et al. in the suspension application to provide non-contact motion control [48]. The sliding mode stress-based controller was developed for a rotary SMA activated manipulator where the system dynamics implemented inside the SMC feed-forward controller was used to calculate the desired

3. LITERATURE REVIEW

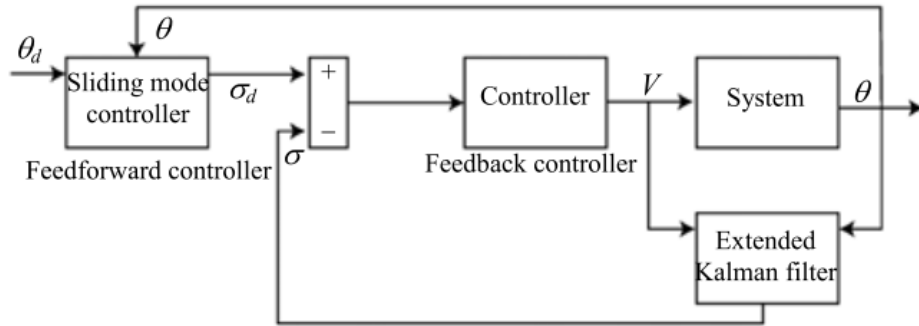


FIGURE 3.2: Sliding model stress based control [49]

stress to obtain the desired position [49]. The controller block diagram of this rotary manipulator system is shown in Figure 3.2. The author concluded feedforward-feedback control system combined with SMC shows high accuracy in tracking and reasonable abilities to deal with uncertainties. The drawback is that sliding model control is application-specific and cannot be used to derive the general control framework.

A Variable Structure Control (VSC) is another nonlinear control algorithm that works in a similar manner to Sliding Mode Control, but it changes the dynamics of a nonlinear system using frequency switching control, instead of the sliding surface. Grant et al. [50] implemented this nonlinear control algorithm in a pair of antagonistic SMA actuators, the feedback of which switches between the actuators, depending on the sign of errors as shown in Figure 3.3 [50]. The VSC algorithm also shows a high accuracy in tracking of the position state and robustness to uncertainties and external disturbance. However, there are a number of the remaining issues discussed by the author, including inability of tracking when an error is large, ringing and chattering.

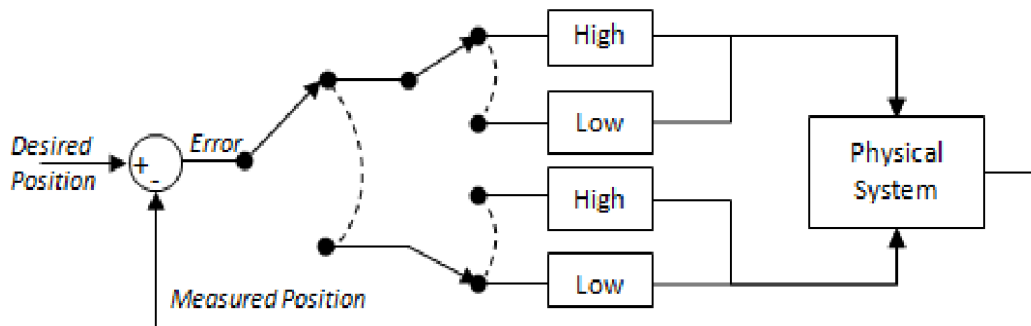


FIGURE 3.3: Variable Structure Control [9] adapted from [50]

3.2.2 Adaptive Control

An Adaptive Control is a modern class of control algorithm, which has the ability to self-tune a controller in stochastic nonlinear systems [51]. This field of control algorithms has been increasing expanded, following the development of computational capabilities in recent years. Examples of such a controller in the shape memory alloy control community include Neural Network Control (NNC) and Fuzzy Logic Control (FLC). A Neural Network Control algorithm has been utilized in many engineering areas to capture the hysteresis characteristics of a mechanical system since in 1990s since it has the properties of nonlinear function mapping and adaptation [51]. Song et al. integrated two neural networks to model both forward and inverse hysteresis relationships between applied voltage and displacement, the structure of which is shown in Figure 3.4.

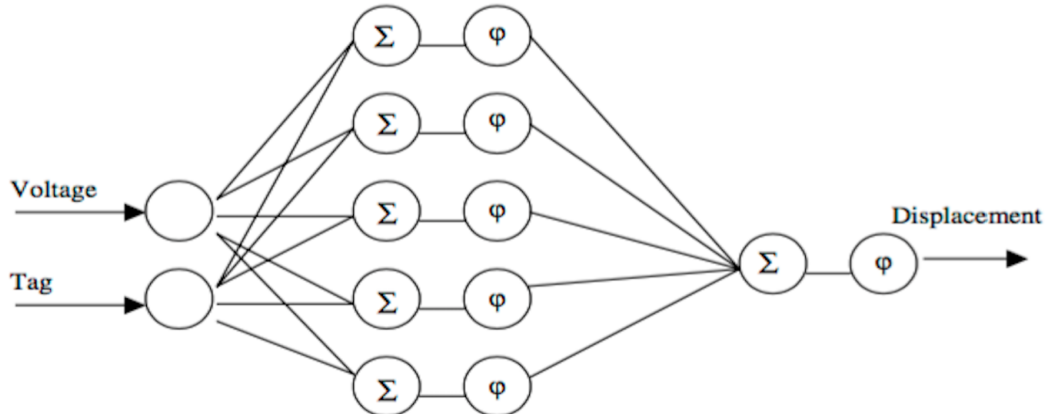


FIGURE 3.4: Schematic of a Neural Network Structure [52]

With the training date generated from experiments, the control algorithm successfully eliminated the need for physical position sensors on the SMA wire actuator system. In the experiments conducted, it was found that the NNC with the inverse model of hysteresis demonstrated reasonable tracking accuracy to sinusoidal reference signal in open loop, proving the effectiveness of the control algorithm. This type of control algorithm is, in fact, an alternative solution to the research question of mitigating uncertainties present in the SMA actuator models. Although a Neural Network Control is an effective algorithm for parameter and controller identification and

3. LITERATURE REVIEW

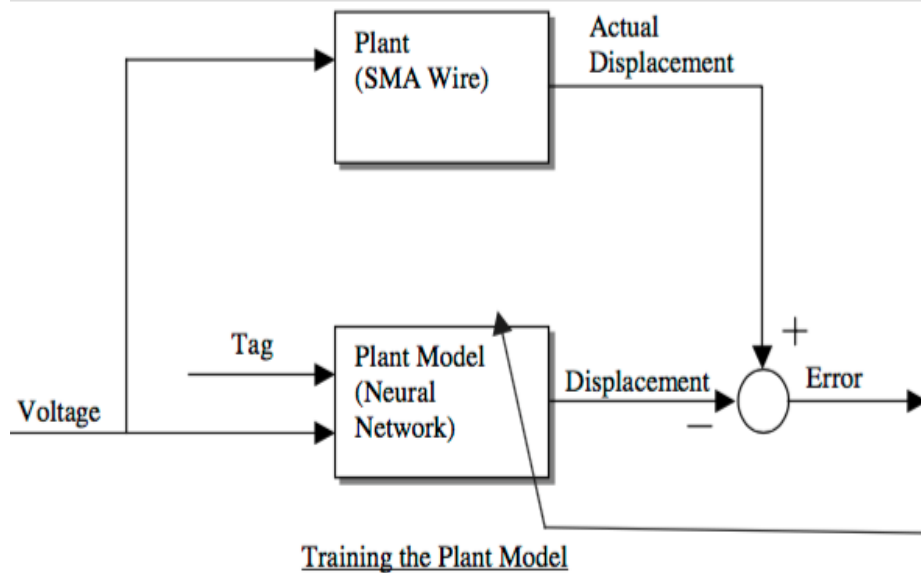


FIGURE 3.5: Schematic of Forward Neural Network training [52]

adaptation to solve the research question, the algorithm requires substantial amount of training data to secure the statistical accuracy of the training data, and the training method/process plays an important role (i.e. in Figure 3.5) as the selected data should be such that it represents the system as much as possible to obtain reasonably accurate results. This means that this control algorithm is application-specific, meaning that the SMA actuator only operates through the NNC under circumstances where the data is collected and can be used to estimate with good accuracy.

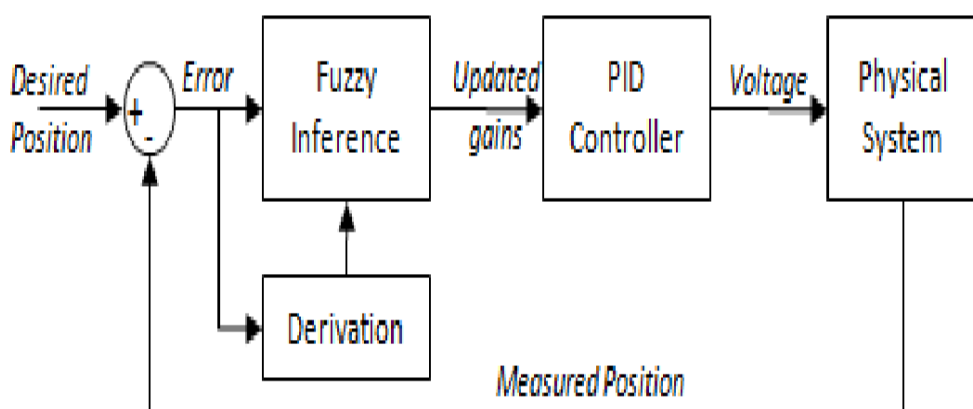


FIGURE 3.6: Fuzzy logic gain adapted PID control [9] adapted from [53]

A Fuzzy Logic Control (FLC) is another adaptive control algorithm for nonlinear systems, which is based on empirically obtained knowledge or data about the system. This control algorithm is also popular in the SMA actuation control research area for hysteresis compensation in nonlinear models. The self-tuning PID controller was developed by Ann et al. [53] in Figure 3.6, including fuzzy inference into the system controller to update the gains of the main PID controller. This was to overcome the nonlinearities and uncertainties in the parameter and operating environments. The author successfully demonstrated better tracking performance of the SMA actuator than using the conventional PID controller [42], while the area of concern is the nature of fuzzy rules, being dependent on, 'rather intuition or practical experience' [9].

3.3 State estimation

In general, the non-model based nonlinear control algorithms provide sufficient solutions to the aforementioned nonlinearity and hysteresis control issues in an application-specific manner. However, most of the control strategies lack of attention to uncertainties in general control framework, especially model parameters, and assume the availability of full information of state variables of a SMA actuated system, which is not always the case where the full potential of a NiTi based SMA actuator is demanded as a compact size and weight minimized actuator. In Chapter 3.2.2, the concepts of Neural Network and Fuzzy Logic Control algorithms were reviewed in the literature , showing that these control methods improve the robustness in model and parameter uncertainties based on the intuitive knowledge of a SMA actuator system. The main drawbacks in these types of non-model based adaptive control algorithms are the need for a large amount of training through simulation and experiments, application-specific, the sensitivity to training methods, and the associated time and cost. Alternatively, some integrated a state observer, namely Kalman filter and its variants, in the controller design to provide solutions to the uncertainty problem.

3.3.1 Kalman Filter

A Kalman filter is a type of state observers or estimators that calculates the estimates of posterior mean and covariance of a state variable recursively over time based on the measurement and dynamic models. The use of a Kalman filter is generally restricted to the linear dynamic systems where the probability density function is Gaussian with unimodal when Gaussian noise is added. These cases are normally not satisfied fully in real situations, and also this is not the case of any SMA actuation systems.

However, Ahn et al. [54] designed the adaptive control algorithm with a Kalman filter to provide an output feedback control for a shape memory alloy actuator. In this research, a Kalman Filter was included to eliminate the output measurement noise and estimate the system state variables based on the compensated control signals from the direct adaptive controller, followed by the approximation in the radial basis function neural network due to nonlinearity and parameter uncertainties. This control algorithm reveals that the position of the SMA actuator can be tracked fairly well (or better than conventional PID controller) to multi-step and sinusoidal reference signals. From the literature, the use of a Kalman filter is rarely seen due to its limited ability in a nonlinear dynamics SMA system, and never seen on its own as a state estimator. The use of a simple Kalman filter would only be justified if the nonlinearities and hysteresis were almost compensated as in [54].

3.3.2 Extended Kalman Filter

An Extended Kalman Filter (EKF) is particularly utilized in the control algorithms of a SMA actuator with the focus on eliminating physical sensors implemented on the shape memory alloy actuator system and incorporating the state variables of a shape memory alloy in the models, which are not easy to measure in practice. From a thorough review of the relevant literature, the first application of Extended Kalman Filter in a shape memory alloy actuator was conducted by Elahinia et al. [12] using input voltage measurement and the measured angular position from sensor to estimate the unmeasured state variables (e.g. temperature and stress) in the SMA based manipulator. The schematic diagram of the EKF design in this work is shown in Figure 3.7. In the design of this EKF, the author selected the state vector as

$x = [\theta, \dot{\theta}, \sigma, T]$ where θ = angular position, $\dot{\theta}$ = angular velocity, T = temperature and σ = stress. The martensitic fraction was not selected as a state of the SMA system since the discrete model utilized calculates it as a function of temperature and stress. All the models were discretized to their corresponding backward difference equations. The Jacobian matrix was derived by using the first order Taylor series expansion and was updated at each iteration. It was also shown that the system converged to the true state variables from experiments in almost any initial conditions tested under measurement and process noises.

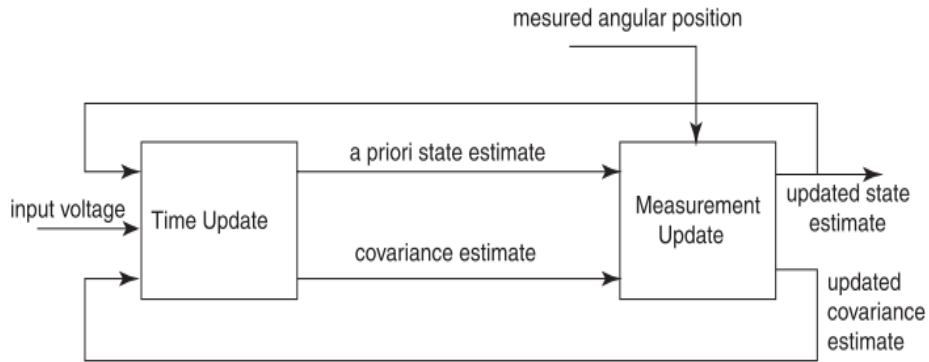


FIGURE 3.7: Schematic of Extended Kalman Filter [12]

Elahinia et al. extended this work to accommodate the complex thermo-mechanical behaviors of a shape memory alloy by feeding back the estimated unmeasured stress and/or temperature into the system since the stress of the SMA device changes due to the motion of the manipulator, and the transformation temperatures also vary slightly due to the change in stress [55]. The author also dealt with these parameter uncertainties by including Sliding Mode control algorithm into stress and temperature based controllers. It was demonstrated that the estimated position state of the SMA system was better matched with the experimental results compared with his initial work in [12]. The literature shows that the use of Extended Kalman Filter is an effective approach to state estimation of unmeasured states of a shape memory alloy based system. However, it was noticed that the computational effort of implementing the state estimation algorithm was ignored, which may become a problem once the dimension of a SMA system becomes large in the large-scaled potential commercial

3. LITERATURE REVIEW

SMA systems.

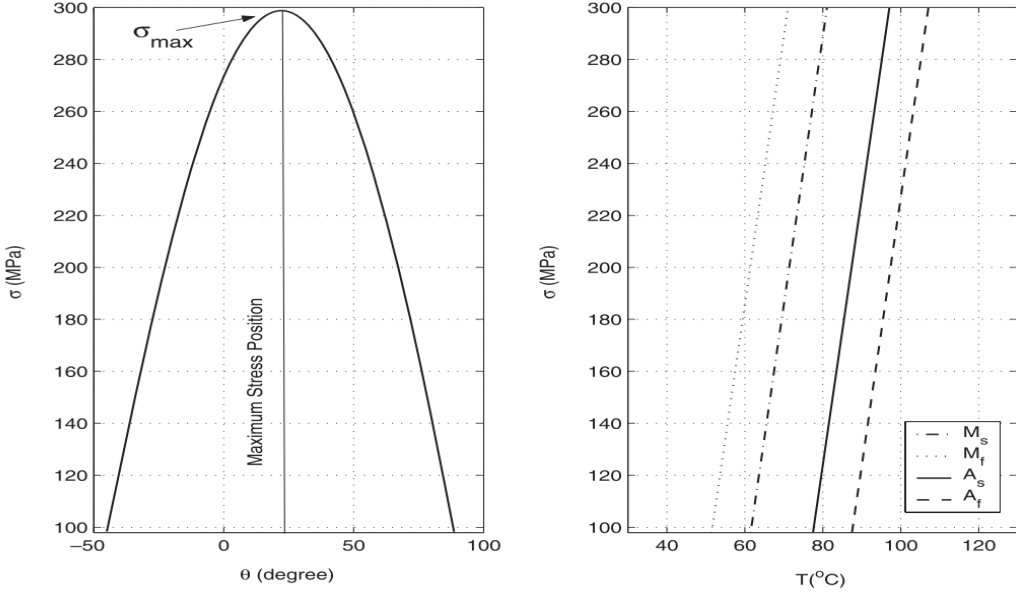


FIGURE 3.8: Transformation temperature dependency on stress [55]

3.3.3 Unscented Kalman Filter

An Unscented Kalman filter has not yet been utilized extensively in the context of shape memory alloy actuators. Recently, Gurung et al. [56] successfully designed the state estimation UKF based algorithm in a simple spring-biased SMA wire actuator. The mean and covariance are obtained using sigma points and passing these points through the actual nonlinear dynamics SMA system provided the accuracy of estimations up to second order for any nonlinear systems considered in this study. The author selected only temperature and stress as the state variables of a nonlinear SMA system. Martensitic phase fraction was calculated based on the posterior stress and temperature from previous time step and then updated in the correction step. The resulting UKF state estimation algorithm was simulated and verified against open-loop experimental results, followed by the comparison against the EKF state estimation results from [57] to sinusoidal signals decreasing in amplitude as shown in Figure 3.9. It can be seen that from the bottom subplot that the error in displacement (e_δ) was reasonably comparable, demonstrating that the UKF performs well in the accurate state estimations, and it

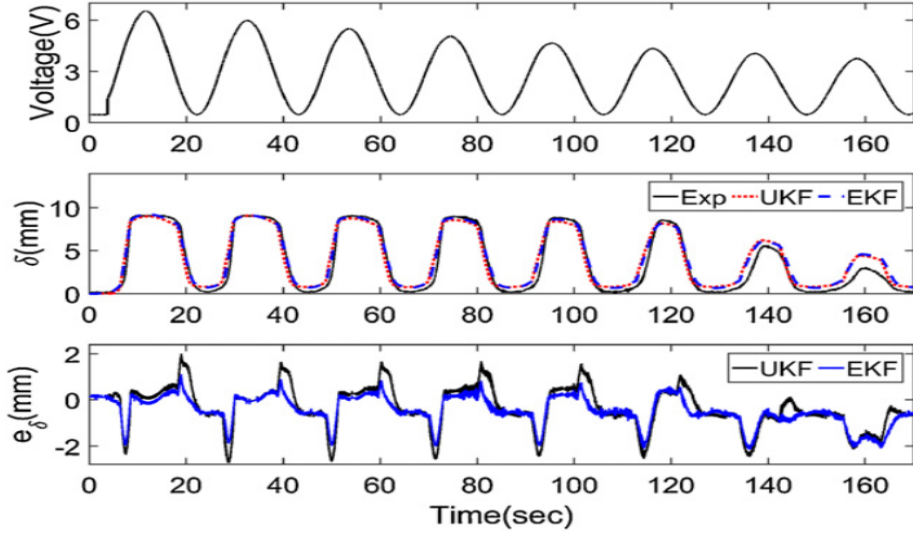


FIGURE 3.9: UKF and EKF performance comparison [56]

was also noted that the computational time consumed by the UKF state estimation algorithm was much less than that by the EKF based algorithm. In this study, the extension to this state UKF technique is taken numerically by integrating the parameter estimation in a Dual Unscented Kalman Filter approach.

3.4 Self sensing control

In general, a sensory feedback is utilized in the control systems of any shape memory alloy actuated systems [45]. The implemented sensors measure thermal, force and strain or displacement position, feeding the knowledges of these states back into the feedback control system for more accurate and robust actuation. Self-sensing control of a SMA based actuator has emerged as a highly demanded research field of control because it eliminates the needs for any external sensors, offering the full potential of a shape memory alloy to work as both sensor and actuator simultaneously. This is especially attractive to the community, requiring miniature actuators such as in biomedical engineering. A self-sensing ability is offered from the accurate modeling of a state of the SMA actuated system, generating the required feedback signal [58]. However, the models of a shape memory alloy usually suffer from significant hysteresis and internal parameters that are difficult to measure and complex thermomechanical behaviors of the alloy, leading to a compromise on the accuracy of the models.

3. LITERATURE REVIEW

As an alternative approach to modeling the complex thermomechanical relationships of a shape memory alloy, the relationship between electric and mechanical properties of a shape memory alloy was investigated extensively, particularly between the electric resistance and strain. It was first proposed by Ikuta et al. [59] in his SMA based servo system by making the resistance-monitoring through the ζ -array configuration (i.e. connecting SMA wires mechanically in parallel, but electrically in series). With the electric resistance feedback, the hysteresis of this shape memory alloy actuator was reduced considerably, which offered accurate enough model to utilize for self-sensing. Several researchers followed this approach [60], [61] and [62], further investigating the electrical resistance and strain relationship under different loading conditions with the focus on the minimization of hysteresis level of a shape memory alloy. Pozzi et al. [61] obtained the results shown in Figure 3.10, depicting the diminishing trend in the hysteresis gap as the SMA is loaded. From Figure 3.10, it can be seen that the resistance-strain relationship is still nonlinear and hysteresis; yet, to the lesser extent, which justifies the idea of using the electric resistance to be self sensed for providing feedback control of displacement of a SMA actuator in a self-sensing manner. The electrical resistance of a shape memory alloy actuator is still to be measured (e.g. using a voltage divider), but it should require less cost, effort and space in practice.

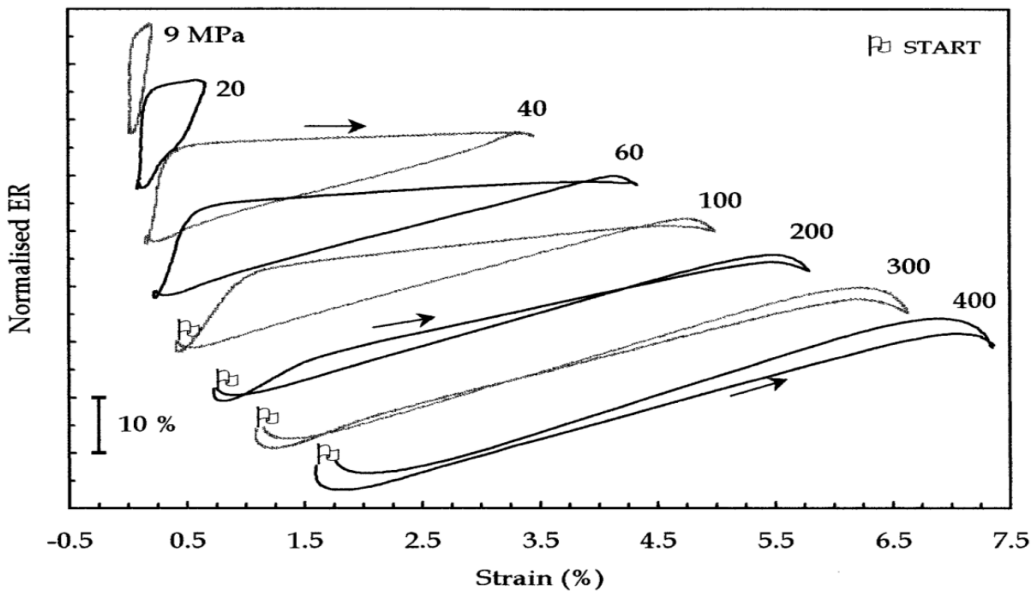


FIGURE 3.10: Hysteresis between electric resistance and strain [61]

The model-based estimation and control algorithm are to be investigated due to its generally high accuracy in tracking control and its independence of any training or a large amount of data required as in non-model-based control algorithms. The accuracy in the control of a shape memory alloy actuator is highly dependent on the accuracy of models of thermomechanical behaviors of a shape memory alloy, which indicates the importance of modeling methods and model parameters. As discussed in Chapter 2, in practical engineering applications, it is common to utilize the phenomenological modeling approach due to its generality of hysteresis treatment, computational efficiency, and the differential and discrete governing equations of the resulting models, which can be handled in an UKF algorithm. Due to the nature of the research question, it is reasonable to select the widely utilized differential governing equations developed by Brinson [63] to represent the dynamics of a spring biased NiTi based shape memory alloy wire actuator described in Chapter 4.1. The established values of parameters of a NiTi shape memory alloy from [63] and [64] are used as nominal values.

4.1 Spring biased SMA wire actuator

In this study, a simple spring biased NiTi shape memory alloy actuator is considered (e.g. one way SME type actuator as presented in Chapter 2.2.1), the graphical repre-

sentation of which is as shown in Figure 4.1.

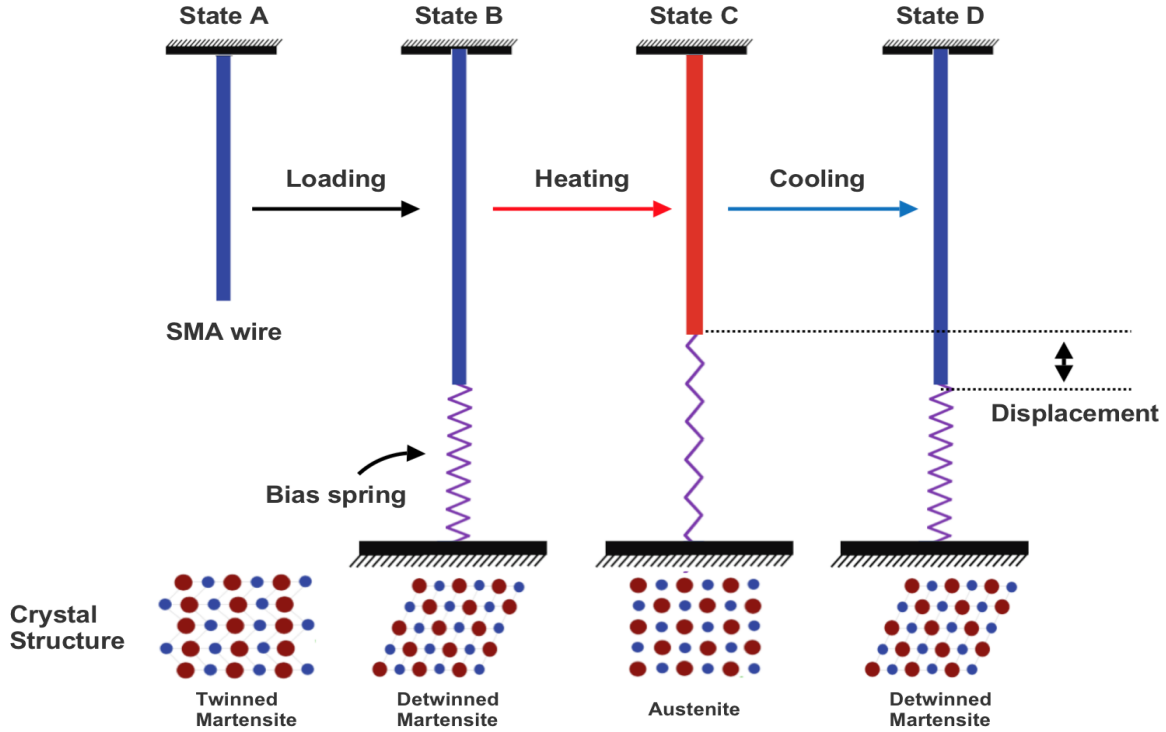


FIGURE 4.1: Working mechanism of a SMA wire actuator

In Figure 4.1, at State A, the shape memory alloy wire is unloaded at room temperature, existing in its twinned martensitic phase. As it is loaded to State B using a bias spring, its phase transforms into its detwinned martensite. Note that in this study, this position is considered as the reference equilibrium position for this type SMA actuator. Upon thermal loading to State C via Joules heating, the SMA wire actuator starts to transform into its high temperature austenitic phase and contracts back to its original unloaded position, resisting bias force from the spring. The difference between State B and C position is taken as a linear displacement by the actuator, which is the variable of interest to control and track in the closed loop control algorithm. As the SMA wire actuator cools down to State D, the bias force of the spring exceeds the restoring force of a shape memory alloy, it goes back to its loaded position (e.g. State B), assuming that a sufficient number of thermal cycles has been conducted to stabilise the permanent strain issue discussed in Chapter 2.3. For continuous operation, the SMA wire actuator undergoes a repeatable

transformation between State B and D, resulting in a linear displacement for actuation.

4.2 Shape memory alloy modelings

The models of a spring-biased SMA actuator consist of a heat transfer, phenomenological phase transformation, constitutive, kinematic and dynamics of the spring biased SMA wire actuator as well as electrical resistance model for the self-sensing purpose. These models are related to each other in the complex nonlinear thermomechanical manner as shown in Figure 4.2.

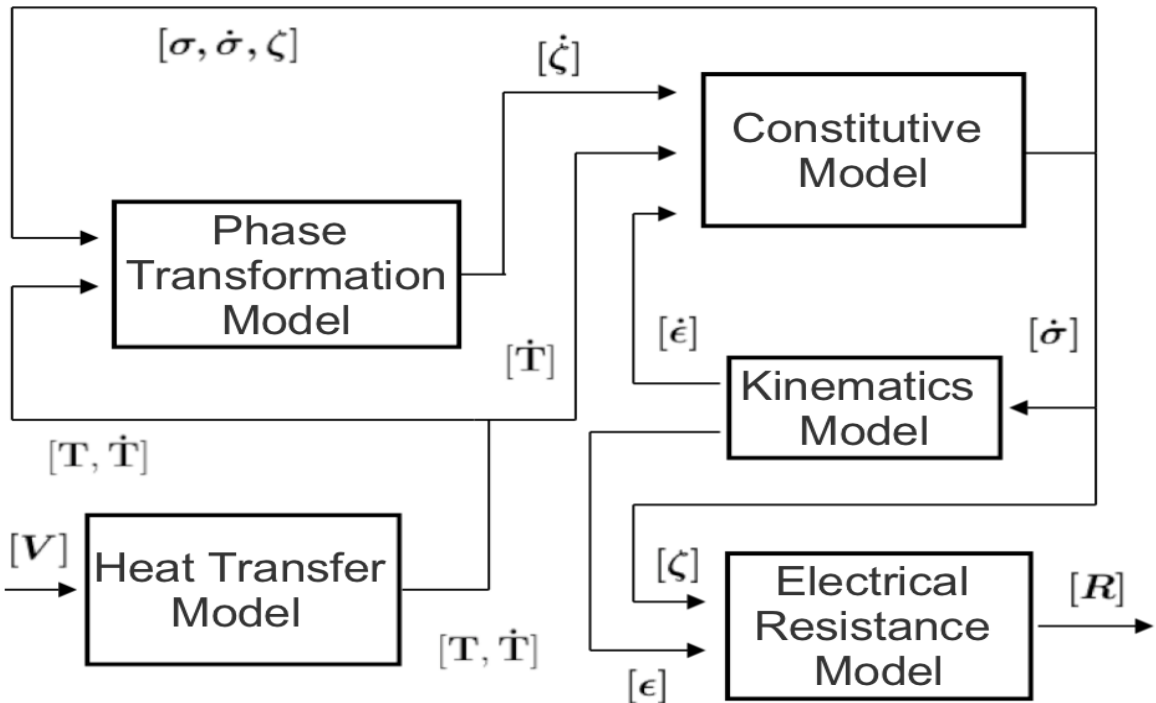


FIGURE 4.2: Schematic diagram of SMA wire actuator

For the purpose of numerical feasibility study of Unscented Kalman Filter based estimations, the simulation results with UKF are compared with the SMA model in Figure 4.2. For each UKF simulation, control input voltage (V) and observed electrical resistance (R) are initially obtained by simulating this nonlinear SMA actuator model, the data of which are then used for the UKF simulations. Hence, in this study, an estimation error at each time iteration is defined by the difference between the

estimated state variable from the UKF state filter and the simulated state collected from the nonlinear model.

4.2.1 Heat transfer model

Since the shape memory alloy wire actuator is activated via Joules heating, the heat transfer relationship of the SMA wire can be modeled as:

$$mC_p \frac{\partial T}{\partial t} = \frac{V^2}{R} - hA_{circ}(T - T_\infty) \quad (4.1)$$

where m = mass per unit length, C_p = specific heat, R = resistance per unit length, A_{circ} = circumference surface area, T_∞ = ambient temperature and h = heat convection coefficient. Note that the heat convection coefficient is approximated by a second order polynomial of temperature for better accuracy where h_0 and h_2 are empirical nominal values, which are the candidates of parameter adaptation.

$$h = h_0 + h_2 T^2 \quad (4.2)$$

This heat transfer model assumes that there are negligible heat conduction and radiation from the SMA actuator. For simplicity, a temperature profile along the SMA wire is assumed constant, meaning that the temperature is uniformly distributed. These are reasonable assumptions, considering the relatively small size of a SMA wire actuator and the small amount of radiative heat transfer. In practice, it is important to ensure for modeling accuracy that the SMA actuator is insulated at its ends to minimize the heat conduction to a wire clamp and the bias spring.

4.2.2 Phase transformation model

To account for hysteresis effects during reverse (martensite \Rightarrow austenite) and forward (austenite \Rightarrow martensite) phase transformation, different phase transformation models are considered upon heating and cooling [63].

$$\zeta = \frac{\zeta_M}{2} [\cos(a_A(T - A_s) + b_A\sigma) + 1] \quad (4.3)$$

Equation 4.3 is the reverse phase transformation model from detwinned martensite to austenite where ζ_M = maximum martensite fraction during cooling, $a_A = \frac{\pi}{A_f - A_s}$, $b_A = \frac{-a_A}{C_A}$ and C_A = curve fitting parameter from the experiments [63].

$$\zeta = \frac{1 - \zeta_A}{2} \cos[a_M(T - M_f) + b_M\sigma] + \frac{1 + \zeta_A}{2} \quad (4.4)$$

Equation 4.4 represents the forward phase transformation from austenite to detwinned martensite during cooling process where ζ_A = minimum martensite fraction during heating, $a_M = \frac{\pi}{M_s - M_f}$, $b_M = \frac{-a_M}{C_M}$ and C_M = curve fitting parameter from the experiments [63].

To integrate into the numerical simulations, Equation 4.3 and 4.4 are differentiated, resulting in the following equations:

$$\begin{aligned} Heating : \dot{\zeta} &= \frac{-\zeta_M}{2} \sin(a_A(T - A_s) + b_A\sigma)(a_A\dot{T} + b_A\dot{\sigma}) \\ &\text{if } A_s < T < A_f, \quad \text{otherwise} \quad \dot{\zeta} = 0 \end{aligned} \quad (4.5)$$

$$\begin{aligned} Cooling : \dot{\zeta} &= \frac{\zeta_A - 1}{2} \sin(a_M(T - M_f) + b_M\sigma)(a_M\dot{T} + b_M\dot{\sigma}) \\ &\text{if } M_f < T < M_s, \quad \text{otherwise} \quad \dot{\zeta} = 0 \end{aligned} \quad (4.6)$$

Once the phase transformation upon either heating or cooling is completed, no subsequent phase transformation occurs beyond the start and finish characteristic transformation temperatures, leading to $\dot{\zeta} = 0$. All the constant parameters were empirically obtained in [63], and taken as nominal values in this study.

4.2.3 Constitutive model

The constitutive model of a NiTi based SMA wire actuator describes the relationship between the rate of internal states of a shape memory alloy, namely strain, stress and temperature, as shown in Equation 4.7.

$$\dot{\sigma} = D(\zeta)\dot{\epsilon} + \Theta\dot{T} + \Omega(\zeta)\dot{\zeta} \quad (4.7)$$

$$\text{where } D(\zeta) = \zeta D_a + \zeta(D_m - D_a) \quad \text{and} \quad \Omega(\zeta) = -\epsilon_l D(\zeta)$$

where D_a = modulus of elasticity of austenite state, D_m = modulus of elasticity of martensite state, Θ = thermal expansion factor and ϵ_l = maximum residual strain. This constitutive model is slightly modified from the original model to take into account the change in the modulus of elasticity during phase transformation [56]. ϵ_l and Θ are both considered as constants as suggested by Brinson [63] due to their relatively small change as a function of ζ , ϵ and T . However, these values are based on the experimentally generated empirical relation for a shape memory alloy in the specific application, which means that the actual values are likely to differ from the nominal constants. This restricts the use of these parameters in only particular situations where a particular thermomechanical load is applied, from which the empirical relations are derived, otherwise bringing an uncertainty in these parameters.

4.2.4 Kinematic and actuator dynamic model

As the SMA wire actuator is heated via Joules heating, the pre-tensioned SMA wire starts to contract while being resisted by the bias spring, which induces the recovery stress in the shape memory alloy. This stress is applied to the bias spring in the same amplitude, extending the spring by displacement δ as expressed in Equation 4.8.

$$\delta = \frac{\sigma A_{cross}}{k_s} \quad (4.8)$$

where A_{cross} = cross sectional area of wire, and k_s = stiffness of the bias spring. The displacement of the spring, δ , corresponds to the actuated linear displacement

of the SMA actuator from the equilibrium (or State B in Figure 4.1. The strain of the SMA actuator can be calculated using a simple stress-strain relationship as in Equation 4.9.

$$\epsilon = \epsilon_0 - \frac{\sigma A_{cross}}{k_s L_0} \quad (4.9)$$

where ϵ_0 = initial strain and L_0 = initial undeformed length of SMA wire. The actuator dynamic is given in Equation 4.9. Equation 4.9 is expressed in its differential form to describe the kinematic behavior of the SMA wire actuator as in Equation 4.10.

$$\dot{\epsilon} = \frac{-A_{cross}}{k_s L_0} \dot{\sigma} \quad (4.10)$$

4.2.5 Electrical resistance model

The electrical resistance of the shape memory alloy wire actuator can be expressed using the general equation for an electrical conductors as expressed in Equation 4.11.

$$R = \frac{\rho_e L}{A_{cross}} = \frac{\rho_e L_0 (1 + \epsilon)}{A_0} \quad (4.11)$$

where ρ_e = electrical resistivity of the SMA actuator and A_0 = initial cross section area of the SMA wire. An electrical resistivity is a materials property, which varies during the phase transformation processes, depending on martensitic phase fraction at each time. Using the same approach for the modulus elasticity of a shape memory alloy from Equation 4.7, the variation in electrical resistivity of a SMA actuator can be expressed as $\rho_e = \zeta \rho_{ea} + \zeta (\rho_{em} - \rho_{ea})$ where ρ_{em} and ρ_{ea} are the electrical resistivity of martensite and austenite state of a shape memory alloy respectively. In this model, it is assumed that the cross sectional area of the SMA wire remains fairly constant at the initial cross section area due to very small change in the cross sectional area. Based on this electrical resistance model, a self-sensing property of the SMA wire actuator is simulated based on the previously described shape memory alloy models in a controlled fashion as in Figure 4.2, which will be then used as a measured observation variable in the UKF estimation algorithms in the following Chapter 4.3.

4.2.6 Summary of SMA model and materials parameters

Table 4.1 below shows the summary of nominal parameters presented in the shape memory alloy wire actuator models. These parameters are determined either from nominal values in the literature [63], [64] or experimental values obtained by the previous undergraduate student at the School of Aeronautical, Mechanical and Mechatronic Engineering, the University of Sydney [65].

Table 4.1: Model and nominal materials properties [63], [64], [65]

Symbol	Value (Unit)	Symbol	Value (Unit)
d	0.6 mm	c_M	10 MPa/ C°
m	1.14×10^{-4} kg/m	ϵ_l	0.067
R	$0.849 \omega/m$	Θ	550 kPa/ C°
h_0	$120 \text{ W}/m^2\text{C}^\circ$	D_m	28 GPa
h_2	$0.001 \text{ W}/m^2\text{C}^\circ{}^3$	D_a	75 GPa
A_{circ}	$4.71 \times 10^{-4} m^2$	A_{cross}	$2.83 \times 10^{-7} m^2$
A_f	78 C°	k_s	100 N/m
A_s	68 C°	L_0	0.25 m
c_A	$12 \text{ MPa}/\text{C}^\circ$	ρ_{ea}	$8.37 \times 10^{-7} \Omega m$
M_f	42 C°	ρ_{em}	$9.60 \times 10^{-7} \Omega m$
M_s	52 C°	C_p	$320 \text{ J}/\text{kg}\text{C}^\circ$
T_∞	20 C°	L_0	0.25 m
ζ_M	1	ζ_A	0

4.3 Dual Unscented Kalman Filter algorithms

As discussed previously in Chapter 2.5, an Unscented Kalman Filter algorithm is a more suitable estimation technique by comparison with other variants of Kalman filtering in highly nonlinear dynamics systems such as the SMA wire actuator considered in this study. This is attributed to the use of a processing method called the Unscented Transformation (UT). The Unscented Transformation allows the UKF to approximate the state distribution by a Gaussian Random Variable (GRV) using a set of carefully chosen

sigma points. These points accurately capture the true mean and covariance of the GRV up to the 2nd order (Taylor series expansion) for any nonlinearity when propagated through an actual nonlinear system [66]. Hence, the UKF achieves a greater estimation performance than an alternative filter such as EKF, whose estimation performance is limited to 1st order due to the truncations of other terms in the Taylor series expansion.

In this study, a Dual Unscented Kalman Filter algorithm is developed for the NiTi based SMA wire actuator in an attempt to study the numerical feasibility of a dual estimation. The dual estimation in this context means the simultaneous estimation of state variables of the SMA wire actuator and parameters used in the SMA models in Chapter 4.2. Consequently, two parallel UKFs are run simultaneously where the estimate of each filter is used in another filter at the current time step [67]. In Chapter 4.3, the basic steps of each estimation algorithm for the SMA actuator are presented, the nonlinear system behaviors of which are represented using the dynamics and corresponding observation model in discrete Equation 4.12 and 4.13 form respectively. The state and parameter estimation filter algorithm are presented in the following Chapter 4.3.2 and Chapter 4.3.3.

$$x_k = f(x_{k-1}, u_{k-1}, q_{k-1}) + w_{k-1} \quad (4.12)$$

$$y_{k-1} = \eta(x_{k-1}, q_{k-1}) + v_{k-1} \quad (4.13)$$

where x_k is the state variable vector at the current time t_k and f is the nonlinear process function evaluated at the previous time t_{k-1} . The control input u_{k-1} and estimated parameter vector q_{k-1} are utilized in the process function along with process noise vector w_{k-1} to consider for modeling error, discretization errors and other uncertainties [66]. y_{k-1} is referred to as the observation vector, which is a nonlinear observation function η with the v_{k-1} measurement noise. In this study, all noises are assumed to be additive (or zero mean) white Gaussian natures for simplicity.

4.3.1 Unscented Transformation

In the propagation of a vector of Gaussian Random Variables with the dimension of n through a nonlinear function, the statistics of the state and observation vector can be calculated using a set of $(2n + 1)$ sigma points represented as χ in Equation 4.14 [66].

$$\begin{aligned}\chi_0 &= \bar{x} \\ \chi_i &= \bar{x} + (\sqrt{(n + \lambda)P_x})_i \quad i = 1, \dots, n \\ \chi_{i-n} &= \bar{x} - (\sqrt{(n + \lambda)P_x})_{i-n} \quad i = n + 1, \dots, 2n\end{aligned}\tag{4.14}$$

where \bar{x} is the mean of a GRV and λ is a scaling factor expressed as $\lambda = \alpha^2(n + \kappa) - n$. The constant α scales the spread of sigma points around the mean \bar{x} with its value normally being set between $1 \times 10^{-4} < \alpha \leq 1$. The constant κ is also a scaling factor, which is either set to 0 or $3 - n$ [66]. These scaling factors are tunable to determine the sigma points.

The sigma points propagating through Equation 4.12 and 4.13 are unscented transformed and then used to approximate the posterior mean and covariance before measurement update step based on the weight coefficients in Equation 4.15.

$$\begin{aligned}W_0^m &= \lambda/(n + \lambda) \\ W_0^c &= \lambda/(n + \lambda) + (1 - \alpha^2 + \beta) \\ W_i^m &= W_i^c = 1/2(n + \lambda) \quad i = 1, \dots, 2n\end{aligned}\tag{4.15}$$

where the super script m and c stand for mean and covariance weights. β is a tuning parameter used to incorporate the prior information about the distribution of a GRV where $\beta = 2$ is optimal for Gaussian distribution [66].

4.3.2 State UKF estimation algorithm

The states of the NiTi based spring biased SMA wire actuator at any time can be expressed in terms of temperature (T), stress (σ) and martensitic phase fraction (ζ). Since the martensitic phase fraction is a function of temperature and stress based on

Equation 4.3 and 4.4, in this study, the temperature and stress are considered as state variables of interest to formulate the state vector x_k in Equation 4.16 for the state UKF algorithm.

$$x = [T \quad \sigma]^T \quad (4.16)$$

From the process w_{k-1} and measurement v_{k-1} noises, the covariance of these noises are determined as $\mathbb{E}[w_{k-1}w_{k-1}^T] = Q_{k-1}$ and $\mathbb{E}[v_{k-1}v_{k-1}^T] = R_{k-1}$ respectively. The mean state and covariance at the first time step are initialized as in Equation 4.17.

$$\bar{x}_0 = \mathbb{E}[x_0] \quad \bar{P}_0 = \mathbb{E}[(x_0 - \bar{x}_0)(x_0 - \bar{x}_0)^T] \quad (4.17)$$

$$x_0 = [20C^\circ \quad 7.07MPa]^T$$

In the UKF estimation algorithm, there are two main steps; namely time and measurement update step presented as follows:

1. Time update step

- a) Initially, the sigma points are calculated according to Equation 4.14. Also, from Equation 4.16, the dimension n of the state vector is 2, which means that 5 sigma points are generated using Equation 4.18.

$$\begin{aligned} \chi_{k-1,0}^+ &= x_{k-1}^+ \\ \chi_{k-1,i}^+ &= x_{k-1}^+ + (\sqrt{(n + \lambda)P_{k-1}^+})_i \quad i = 1, \dots, n \\ \chi_{k-1,i}^- &= x_{k-1}^+ - (\sqrt{(n + \lambda)P_{k-1}^+})_{i-n} \quad i = n + 1, \dots, 2n \end{aligned} \quad (4.18)$$

where $+$ indicates after measurement step, while $-$ means before. The posterior mean and covariance from the previous time step are used to generate the sigma points.

- b) Based on the SMA actuator models in Chapter 4.2, a nonlinear discrete process function in the form of Equation 4.12 is to be determined to unscented transform the sigma points. Using differential Equation 4.1 and 4.7 explicitly, the SMA models can be discretized into the following nonlinear process function.

$$\chi_k^- = f(\chi_{k-1}^+, u_{k-1}, q_{k-1}) = \begin{bmatrix} T_k^- \\ \sigma_k^- \end{bmatrix} = \begin{bmatrix} T_{k-1}^- + \frac{\partial T}{\partial t} \Delta t \\ \sigma_{k-1}^- + \frac{\partial \sigma}{\partial t} \Delta t \end{bmatrix} \quad (4.19)$$

$$\chi_k^- = f(\chi_{k-1}^+, u_{k-1}, q_{k-1}) = \begin{bmatrix} T_{k-1}^- + \frac{\frac{V^2}{R} - hA_{circ}(T_{k-1} - T_\infty)}{mC_p} \Delta t \\ \sigma_{k-1}^- + \frac{\Theta \dot{T}_{k-1} + \Omega \dot{\zeta}_{k-1}}{1 + \frac{A_{cross}B}{k_s L_0}} \Delta t \end{bmatrix}$$

where Δt is the time step size in simulations. The explicit method is selected due to its relatively ease of implementation at the cost of a slightly more computational time [57].

- c) Using the unscented transformed a priori sigma points, the a priori mean and covariance of the state variables are obtained according to the weight coefficient in Equation 4.15 as follows:

$$x_k^- = \sum_{i=0}^{2n} W^m(i) \chi_k^- \quad (4.20)$$

$$P_k^- = \sum_{i=0}^{2n} W^c(i) [\chi_k^- - x_k^-] [\chi_k^- - x_k^-]^T + Q_k \quad (4.21)$$

2. Measurement update step

- a) At the start of measurement step, using Equation 4.9 and 4.11, a discrete nonlinear observation function in the form of Equation 4.13 is derived as in Equation

$$Y_k^- = \eta(\chi_k^-, q_{k-1}) = \frac{(\zeta \rho_{em} + \rho_{ea}(1 - \zeta)) L_0 (1 + \epsilon_0 - \frac{\sigma A_{cross}}{k_s L_0})}{A_{cross}} \quad (4.22)$$

Equation 4.22 provides the estimate for an observed variable or resistance of the SMA wire actuator in this study from self-sensing property.

- b) The sigma points passed through Equation 4.22 are then used to obtain the a priori measurement estimate using Equation 4.23.

$$y_k^- = \sum_{i=0}^{2n} W^m(i) Y_k^- \quad (4.23)$$

Likewise, the covariance and cross covariance of the estimated measurement are derived using the following equations respectively.

$$P_{yy}^+ = \sum_{i=0}^{2n} W^c(i) [Y_k^- - y_k^-] [Y_k^- - y_k^-]^T + R_k \quad (4.24)$$

$$P_{xy}^+ = \sum_{i=0}^{2n} W^c(i) [\chi_k^- - x_k^-] [Y_k^- - y_k^-]^T \quad (4.25)$$

- c) The mean and covariance of the state variables are updated in Equation 4.29 and 4.30 using the measured resistance data y_k (or simulated from the SMA model) and a Kalman gain calculated in Equation 4.26.

$$K_k^+ = P_{xy}^+ P_{yy}^{+^{-1}} \quad (4.26)$$

$$x_k^+ = x_k^- + K_k^+ (y_k - y_k^-) \quad (4.27)$$

$$P_k^+ = P_k^- - K_k^+ P_{yy}^+ K_k^{+T} \quad (4.28)$$

- d) Since the UKF algorithm is recursive, at the end of each recursive estimation iteration, the mean and covariance of the state vector are updated for the next iteration in time as follows.

$$x_{k-1}^+ = x_k^+ \quad (4.29)$$

$$P_{k-1}^+ = P_k^+ \quad (4.30)$$

Note that in the UKF filter, the estimated parameter vector q_{k-1} is taken from the parameter UKF filter at the previous time step t_{k-1} , which is not updated, but remains constant in the state filter.

4.3.3 Parameter UKF estimation algorithm

Any parameters used in the SMA models in Chapter 4.2 can be a candidate for parameter estimation if it is expressed in the form of Equation 4.31 [68].

$$q_k = q_{k-1} + w_{q,k-1} \quad (4.31)$$

$$y_k = \tau(x_{k-1}, q_k) + v_{q,k}$$

Similarly to the UKF state filter algorithm, the parameter UKF is first initialized with the mean and covariance of the estimated parameter vector as follows.

$$\bar{q}_0 = \mathbb{E}[q_0] \quad \bar{P}_{q,0} = \mathbb{E}[(q_0 - \bar{q}_0)(q_0 - \bar{q}_0)^T] \quad (4.32)$$

The difference in the time and measurement update step from the UKF state estimation algorithm is highlighted as shown below.

1. Time update step

- a) The sigma points are calculated based on Equation 4.33 in the same form as that in the UKF state filter where n and λ are the same as before. Also, the same weight coefficients derived in Equation 4.15 are incorporated into the parameter UKF estimator.

$$\begin{aligned} Q_{k-1,0}^+ &= q_{k-1}^+ \\ Q_{k-1,i}^+ &= q_{k-1}^+ + (\sqrt{(n + \lambda) P_{q,k-1}^+})_i \quad i = 1, \dots, n \\ Q_{k-1,i}^+ &= q_{k-1}^+ - (\sqrt{(n + \lambda) P_{q,k-1}^+})_{i-n} \quad i = n + 1, \dots, 2n \end{aligned} \quad (4.33)$$

- b) The time update process of the estimated parameter vector q_k^- is performed using the following relation in Equation 4.34 as opposed to using a nonlinear process function in the UKF state filter.

$$q_k^- = q_{k-1}^+ \quad P_{q,k}^- = P_{q,k-1}^+ + Q_{q,k} \quad (4.34)$$

2. Measurement update step

- a) The same discrete nonlinear observation function is used in the parameter UKF filter, except that it is now based on the transformed sigma points of the parameter vector as well as the predicted state vector from the previous time step t_{k-1} .

$$Y_k^- = \tau(x_{k-1}, Q_k^-) = \frac{(\zeta\rho_{em} + \rho_{ea}(1-\zeta))L_0(1 + \epsilon_0 - \frac{\sigma A_{cross}}{k_s L_0})}{A_{cross}} \quad (4.35)$$

The sigma points passed through Equation 4.35 are similarly used to determine the a priori measurement estimate using Equation 4.23.

- b) The covariance and cross covariance of the estimated parameter vector are also derived in Equation 4.36 and 4.37. The measurement update for the posterior mean and covariance of the parameter vector is conducted through the approximated Kalman gain in Equation 4.38 in the same approach as the state UKF filter.

$$P_{yy}^+ = \sum_{i=0}^{2n} W^c(i)[Y_k^- - y_k^-][Y_k^- - y_k^-]^T + R_{q,k} \quad (4.36)$$

$$P_{qy}^+ = \sum_{i=0}^{2n} W^c(i)[Q_k^- - q_k^-][Y_k^- - y_k^-]^T \quad (4.37)$$

$$K_{q,k}^+ = P_{qy}^+ P_{yy}^{+1} \quad (4.38)$$

$$q_k^+ = q_k^- + K_{q,k}^+(y_k - y_k^-) \quad (4.39)$$

$$P_{q,k}^+ = P_{q,k}^- - K_{q,k}^+ P_{yy}^+ K_{q,k}^{+T} \quad (4.40)$$

In summary to Chapter 4.3, the overall schematic diagram of the Dual Unscented Kalman Filter algorithm presented is shown in Figure 4.3. The inputs to the estimation algorithm include control voltage input u_{k-1} (or V_{k-1}) and the self-sensed electrical resistance observation y_K (or R_k), while the outputs from the DUKF are the estimated state and parameter vectors if the two UKFs are run simultaneously. The relevant parameters used in this UKF algorithm are as summarized in Table 4.2.

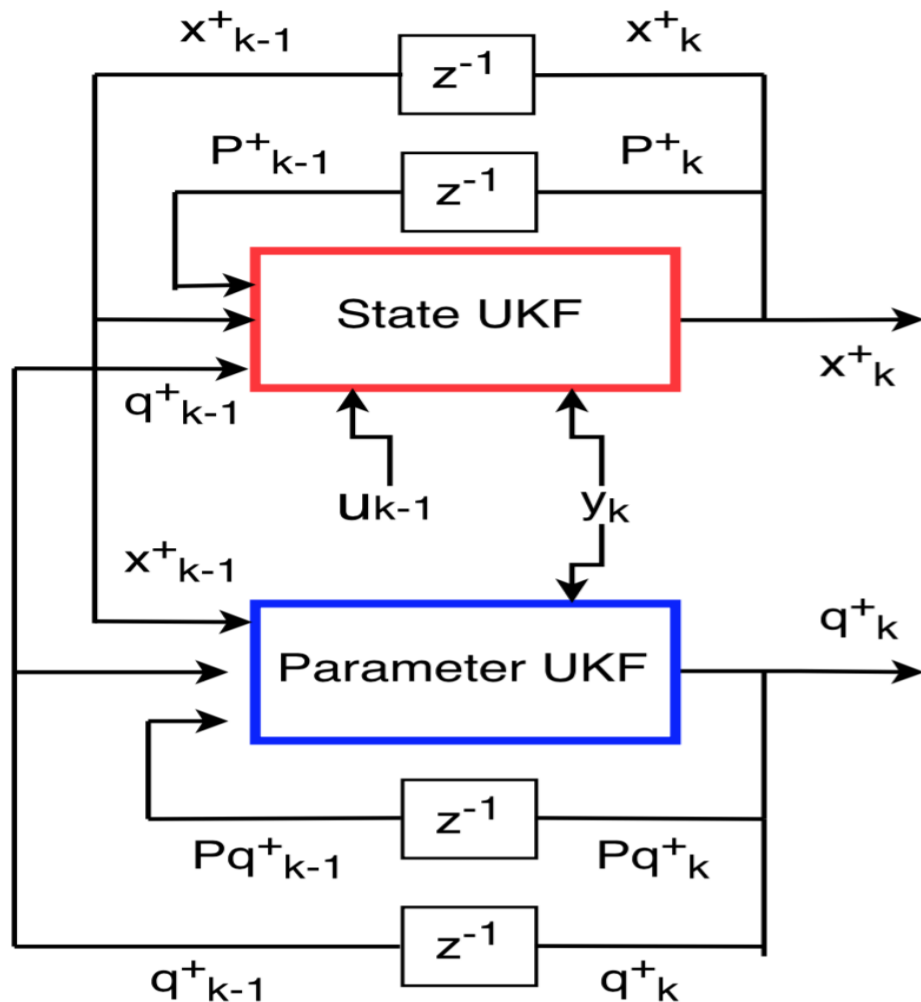


FIGURE 4.3: Schematic diagram of Dual Unscented Kalman Filter algorithm

Table 4.2: UKF filter parameters

Symbol	Value (Unit)	Symbol	Value (Unit)
n	2	α	0.01
β	2	κ	1
Q_k	$10^{-6} I_{2x2}$	$Q_{q,k}$	10^{-6}
R_k	10^{-4}	Δt	10^{-4} s

4.4 Closed loop control

Based on the self-sensing electrical resistance model in Chapter 4.2.5 and the UKF state estimation algorithm presented in Chapter 4.3.2, it is reasonable to construct a closed-loop control algorithm to provide a means for the active precise positioning ability of the SMA wire actuator in practical applications. The overview of the closed-loop control algorithm is as shown in Figure 4.4.

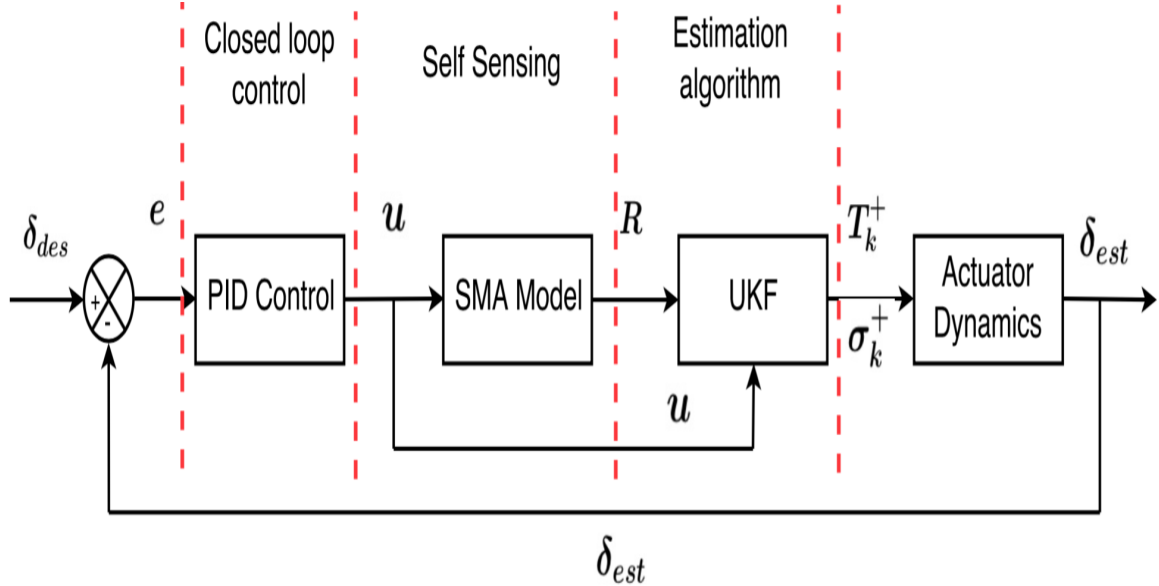


FIGURE 4.4: Overview of the UKF based closed-loop control block diagram

In Figure 4.4, the displacement of the NiTi based SMA wire actuator is to be actively controlled based on a simple Proportional-Integral-Derivative (PID) feedback controller. At any time, a displacement state of the actuator is calculated using the actuator dynamics model in Equation 4.8, which relies on the estimated state vector

from the state UKF. As mentioned previously, the control input voltage (V) and self-sensed electrical resistance (R) are obtained by simulating the shape memory wire actuator model in Figure 4.2, which are then fed into the UKF algorithms. This self-sensing section can be replaced instead with a simple voltage divider as shown in Figure 4.5 [57]. Using the voltage divider, the electrical resistance of a SMA wire can be calculated using the following relation in Equation 4.5.

$$R_{SMA} = \frac{V_s}{V_t - V_s} R_0 \quad (4.41)$$

where V_s and V_t are the voltage across a SMA actuator and total voltage drop respectively with the known resistance of R_0 . With this approach, the SMA actuator achieves a self-sensing without any additional physical sensors.

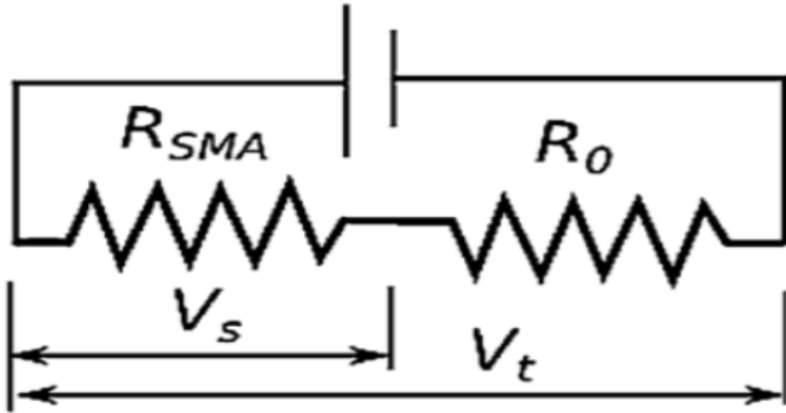


FIGURE 4.5: An example of practical electrical resistance measurement methods [57]

4.4.1 PID controller design

A PID controller is one of the simplest feedback control forms, the basic structure of which is as shown in Figure 4.6. The performance of closed-loop control is governed by three gain terms; namely Proportional, Derivative and Integral gain. The Proportional term feeds back on the current error, pulling the controlled output towards the desired state, while the Derivative term can improve the transient dynamic response of the controlled system by damping oscillatory responses. The Integral term feeds back on the accumulated previous errors, which allows it to eliminate the steady state error in a closed-loop control system. This type of closed-loop controller is integrated into the

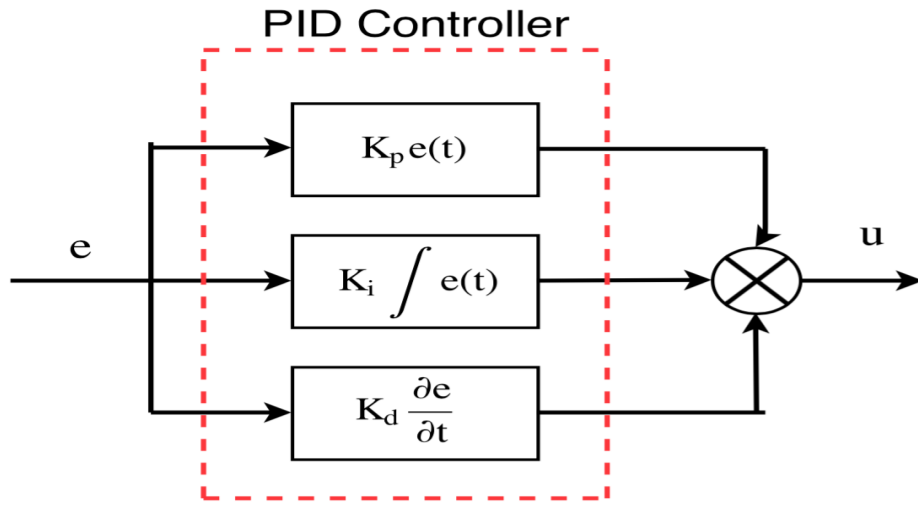


FIGURE 4.6: A schematic diagram of PID controller

overall system in Figure 4.4, feeding back the displacement error between the desired and estimated state. The PID controller gains used in this study are as summarized in Table 4.3.

Table 4.3: PID controller gains

Symbol	Value (Unit)	Symbol	Value (Unit)
K_p	100	K_d	5
K_i	50		

All simulations presented in Chapter 5 have been implemented and performed using MathWorks® MATLAB R2016b and Simulink platform.

5.1 SMA model validation

In this chapter, the shape memory alloy models developed in Chapter 4.2 has been implemented to validate the numerical functionality of the models. For the model validation, the relationship between temperature and strain is plotted as shown in Figure 5.1 to compare against the experimental relation in Figure 2.3. As can be seen, the reverse and forward phase transformations take place at the characteristic transformation temperatures summarized in Table 4.1, resulting in a different path upon heating and cooling. The temperature hysteresis is also well captured, being slightly larger than that from the experimental result in Figure 2.3. However, since all general features mentioned in Chapter 2.1 and 2.3 are observed, it is reasonable to conclude that the SMA models are validated for further simulations.

5.2 State UKF performance analysis

To initially investigate the correctness of numerical implementation of an Unscented Kalman Filter algorithm, only the performance of the state UKF is considered in

5. RESULTS

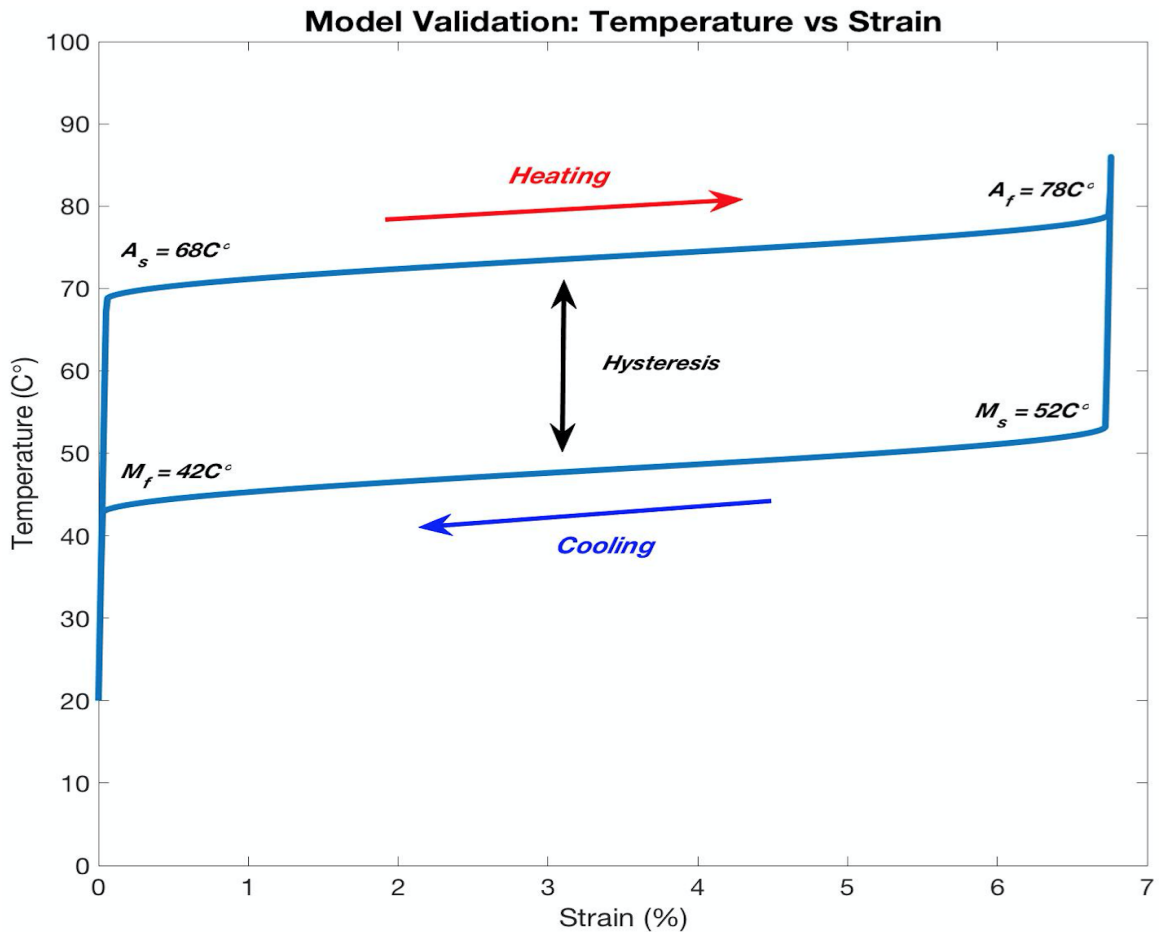


FIGURE 5.1: Model validation - temperature vs strain

Chapter 5.2 using two different voltage input profiles in an open-loop manner. Hence, this is essentially based on the schematic model presented in Figure 4.4 without the PID controller for the closed-loop feedback control, but instead an input voltage is specified. For each UKF simulation, this input voltage and self-sensed electrical resistance through Equation 4.11 are collected by simulating the nonlinear SMA model and used in the state UKF filter. The performance of state estimation is determined by the difference between the nonlinear SMA actuator model and the estimated states in the UKF.

5.2.1 Single square wave

Given the single voltage square wave with a pulse width of 0.5s and the peak voltage of 4V, the following results are obtained in Figure 5.2. The estimated state variables (i.e. temperature and stress) show very accurate matches with those with those obtained from the SMA models. The estimated state variables remain very close to the states from the nonlinear SMA model, resulting in relatively small displacement errors with the peak of 0.009mm. This peak displacement error occurs at the time corresponding to the peak phase transformation rate. This is the expected result because this is where the highest nonlinearity is observed, meaning that the relatively higher displacement error occurs at this time. A smaller phase transformation rate after the peak implies a slower rate of forward phase transformation due to the limited cooling ability of a shape memory alloy. From the phase fraction plot in Figure 5.2, it can be seen that the martensitic phase fraction goes from 1 to 0 upon heating, indicating that the full phase transformation occurs. Hence, it is observed that the state UKF filter provides a sufficiently accurate state estimation for the full reverse and forward transformation, which is typical in actuator applications.

5.2.2 Sinusoidal wave

In addition to the single pulse wave, a sinusoidal voltage profile is also generated to test the performance of the state UKF algorithm. Similarly, a very accurate match with the nonlinear SMA model is observed in the temperature and stress plots in Figure 5.3, leading to even smaller estimation errors as can be confirmed from the smaller magnitude of displacement errors. By comparison, the estimation errors are more spread over time and similar in magnitude due to the slower rate of phase transformation. This slower rate is due to the slower rate of temperature increase via Joules heating. As opposed to the single square wave case, the shape memory alloy only achieves the partial phase transformation; yet, the state UKF filter still holds a good agreement with the nonlinear SMA model, indicating that it is capable of providing the accurate state estimation regardless of phase transformation completion.

Overall, combined with the results from Chapter 5.2.1, it is observed that the estimation performance of the state UKF is numerically confirmed graphically in Figure 5.2 and 5.3.

5. RESULTS

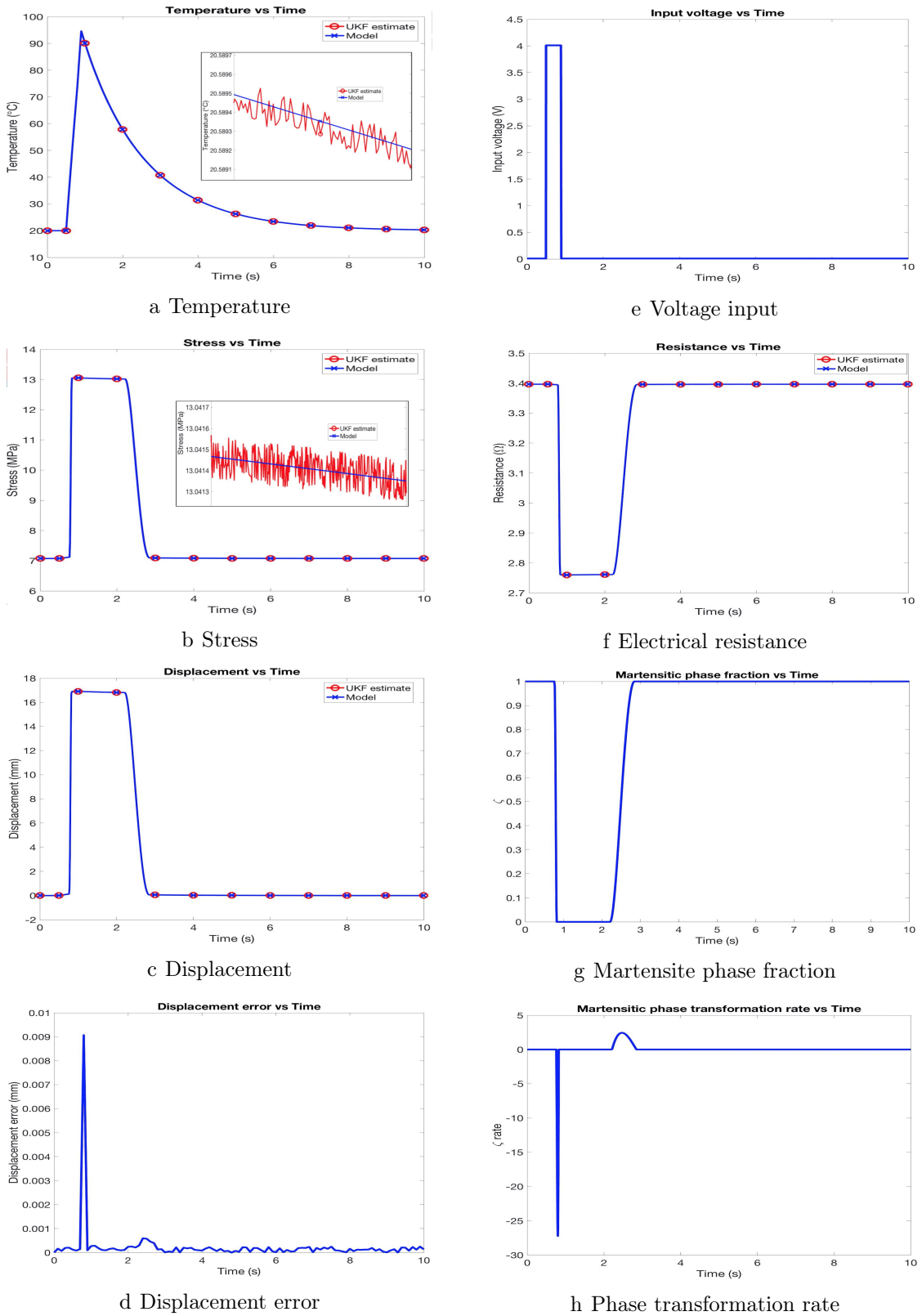


FIGURE 5.2: State UKF estimation to single square voltage wave

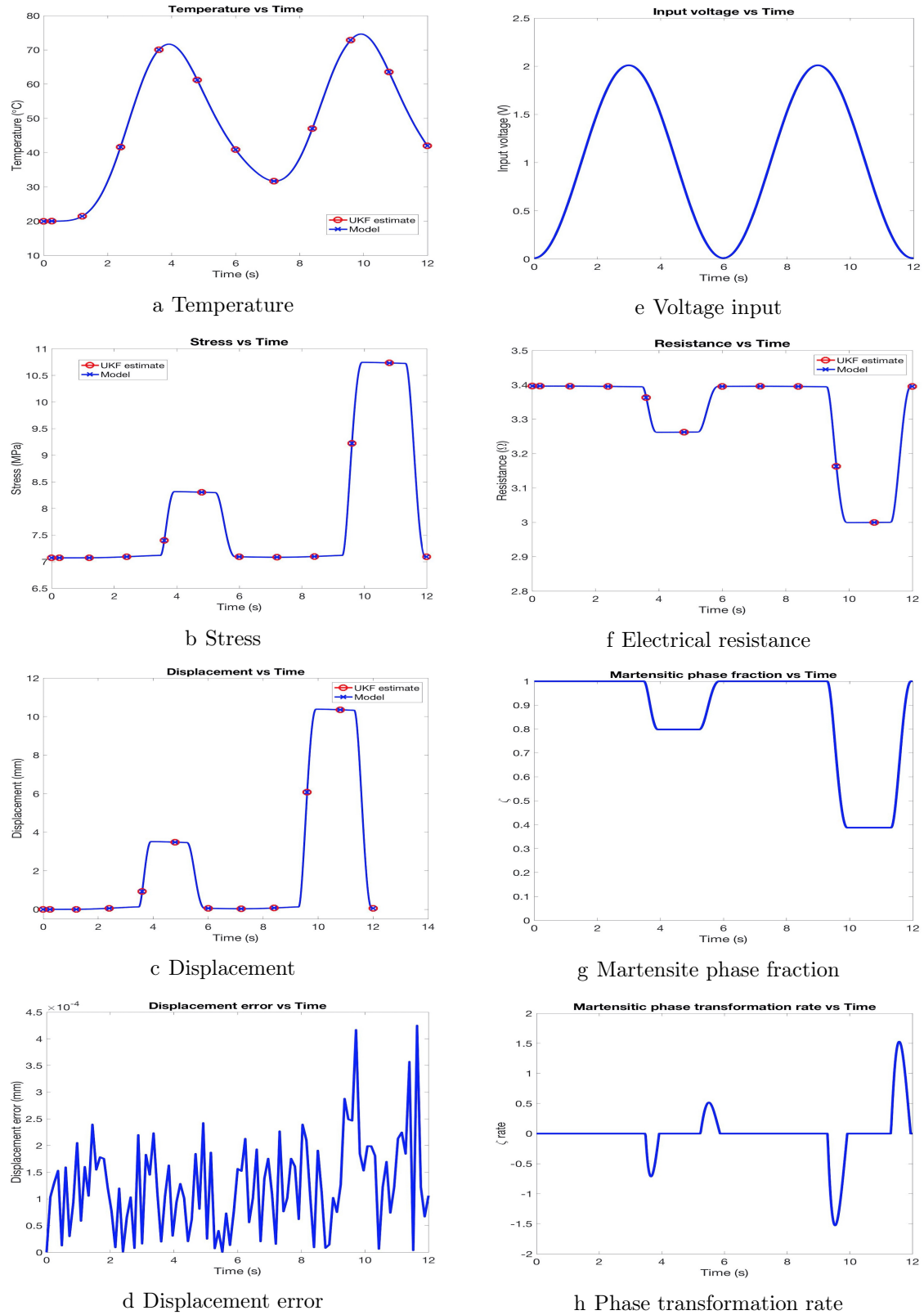


FIGURE 5.3: State UKF estimation to sinusoidal wave

5.3 Realistic noise analysis

In order to simulate a more realistic scenario, a random white Gaussian noise is added to the self-sensing electrical resistance model in addition to the noise covariances as shown on the resistance plot in Figure 5.5. From the temperature and stress plots, it is noticed that the variation in the estimated states is more pronounced with noisier electrical resistance measurements from the nonlinear SMA model, while the estimated states still remain within an acceptable range. This causes a much larger estimation error, leading to the displacement error of up to 0.3mm than those in Figure 5.2 and 5.3. However, this is still about 2% of the total displacement of about 17mm achieved, indicating the high potential of an accurate state estimation by the UKF, even in practical applications.

5.4 Robustness to external disturbance

From time to time, during the operation of the SMA wire actuator, it experiences a range of unexpected external disturbances such as a sudden air blow and mechanical vibrations. The performance of the state UKF filter to reject these disturbances is tested, using an approximated wind gust in the form of a Gaussian distribution in Figure 5.4 as opposed to the more realistic Weibull distribution for simplicity. It is assumed that the temperature drop profile by a wind gust is similar in the distribution nature to that of the wind speed in Figure 5.4.

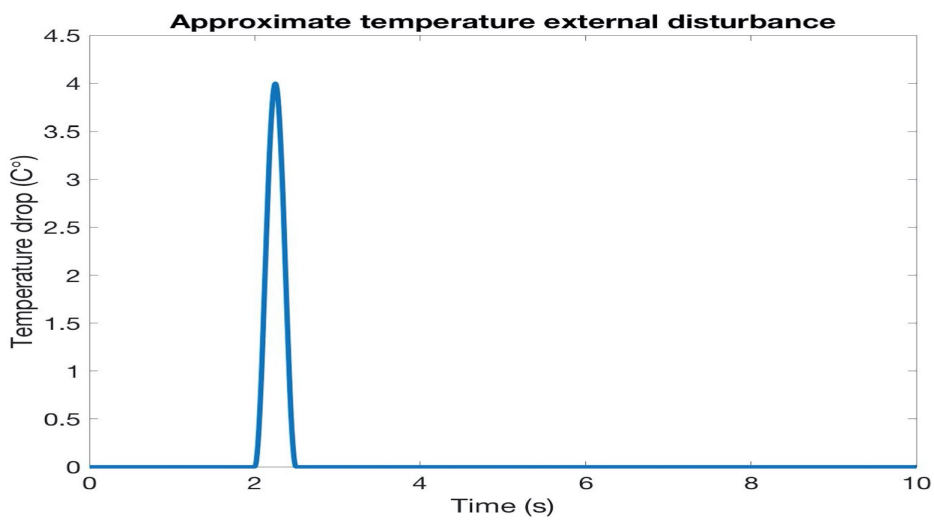


FIGURE 5.4: Approximate temperature external disturbance profile

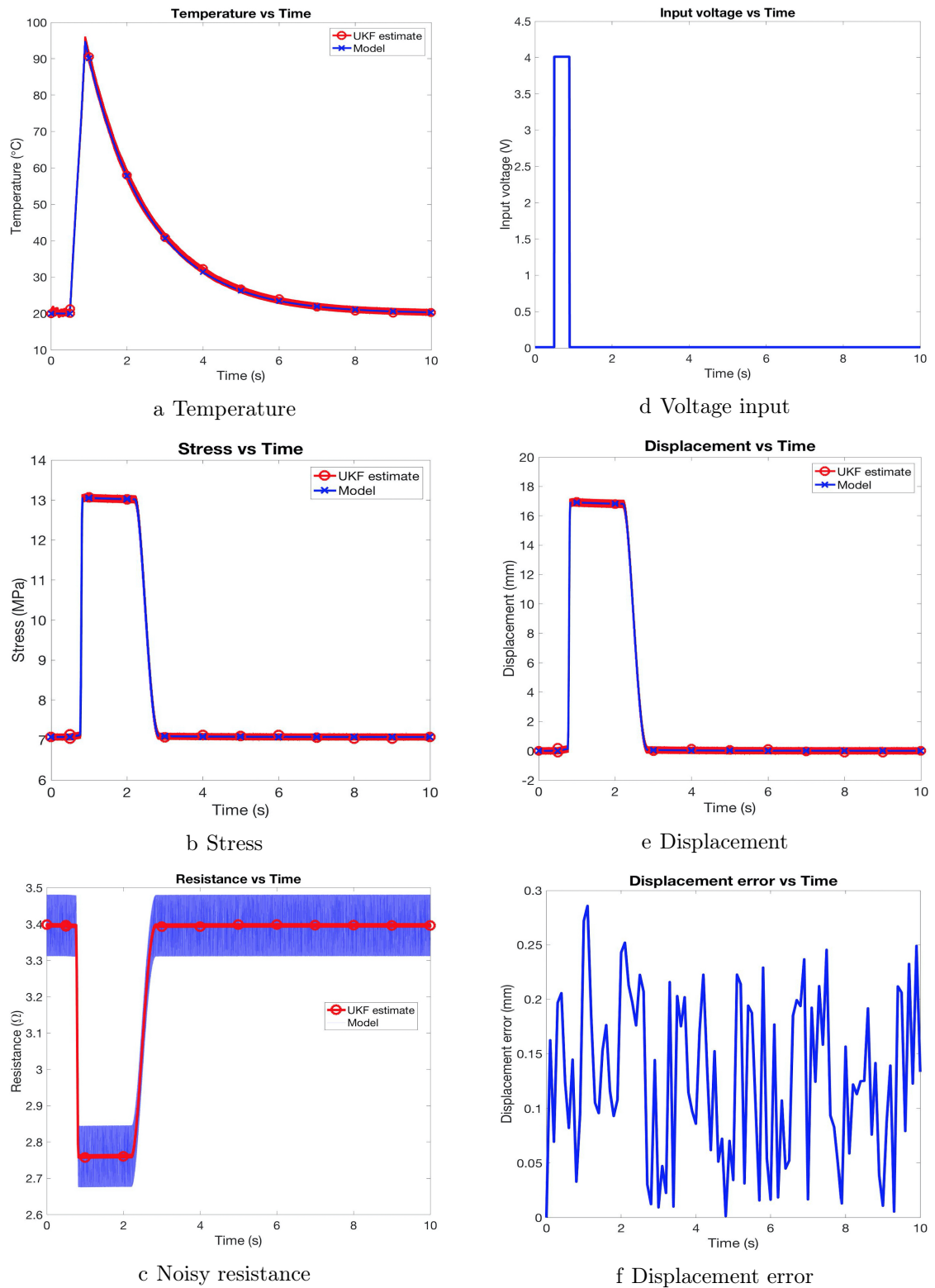


FIGURE 5.5: State UKF estimation under noisier condition

5. RESULTS

For this disturbance rejection analysis, the single square input wave is considered as in Figure 5.2. From Figure 5.6, it can be seen that under the sudden temperature drop from 2s, the state UKF filter still manages to provide a reasonably accurate temperature estimate, resulting in a displacement error lower than its peak where the phase transformation rate is the highest. This shows the evidence of robustness of the state UKF filter to an external disturbance, which supports the use of this estimation algorithm in practice.

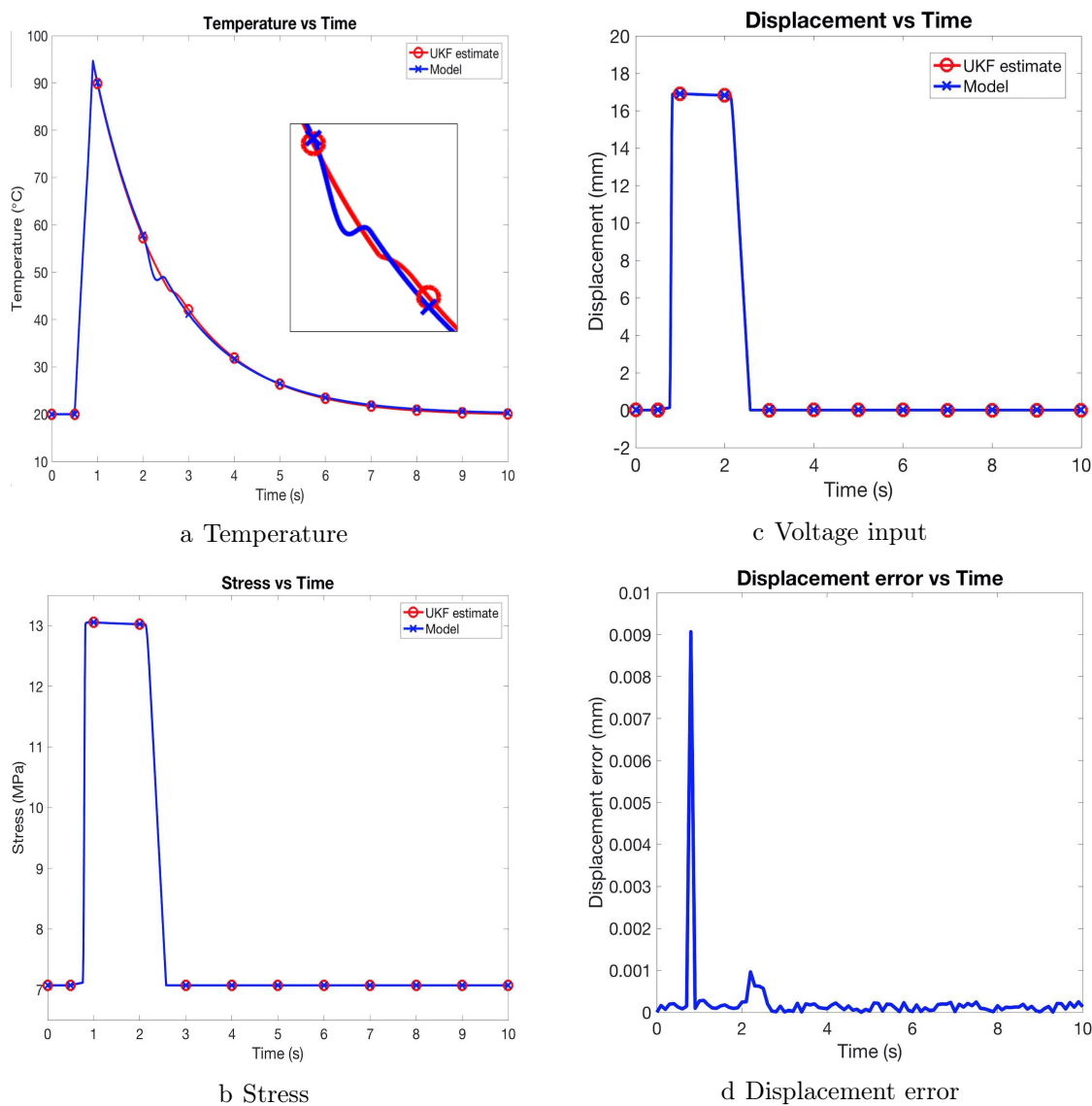


FIGURE 5.6: State UKF estimation with external disturbance

5.5 Parameter UKF performance analysis

Along with the state UKF algorithm, the parameter UKF is run simultaneously to provide the parameter estimate in the dual configuration as presented in Chapter 4.3. In this study, the empirically derived convective heat transfer coefficient term h_0 and thermal expansion factors are selected as the candidate parameters for the parameter estimation by the UKF. This is because these parameters are difficult to measure and calibrate in practice (in other words, these parameters contain uncertainties), and often rely on the nominal values in the literature in the model-based control approaches for a shape memory alloy actuator. Also, the parameters are time-varying due to thermal fatigue and very sensitive to what may not be clearly known (e.g. elemental composition, the number of cycles operated and processing methods).

The performance of the parameter UKF is investigated by observing the convergence of estimated parameters to the nominal values summarized in Table 4.1 from different initial conditions. The initial conditions are taken between $\pm 10\%$ from the nominal values.

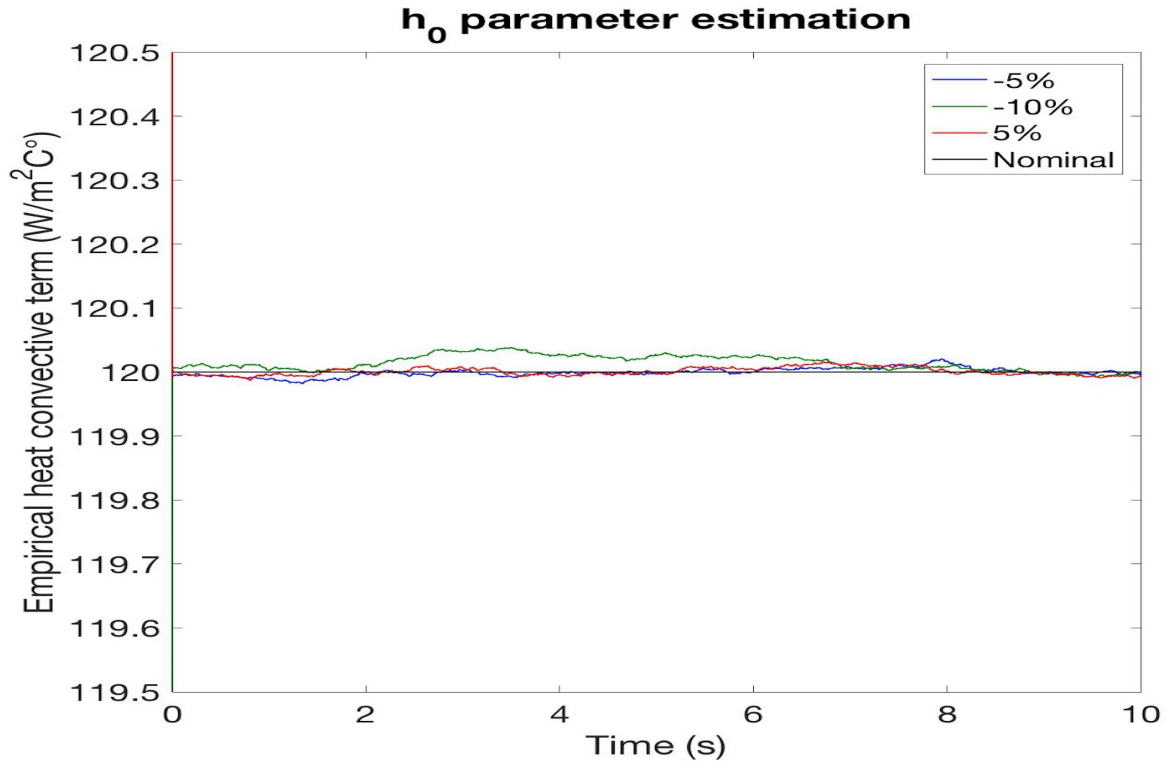


FIGURE 5.7: Empirical convective heat transfer coefficient UKF estimation

5. RESULTS

From Figure 5.7, it is clear that the parameter converges well close to the nominal value after about 8s from three different initial conditions. The general trend is observed between -5 and -10%) that the further away the initial condition is from the nominal value, the longer it takes to converges (or even diverges). This could be the reason why the estimated thermal expansion factor does not converge as well as the convective heat transfer coefficient in Figure 5.8. Although it converges towards the nominal value as can be seen from the $\pm 5\%$ nominal value, there is a noticeable estimation error even at 20s. This may suggest that for some parameters, it may take much longer time to provide the accurate estimated values or really good initial estimates are necessary for the sufficiently accurate estimation in a reasonable amount of time. However, the parameter UKF algorithm can be still said that it provides a good evidence for parameter estimations based on the result in Figure 5.7 and it can be run prior to the operation of the SMA wire actuator for parameter identification offline.

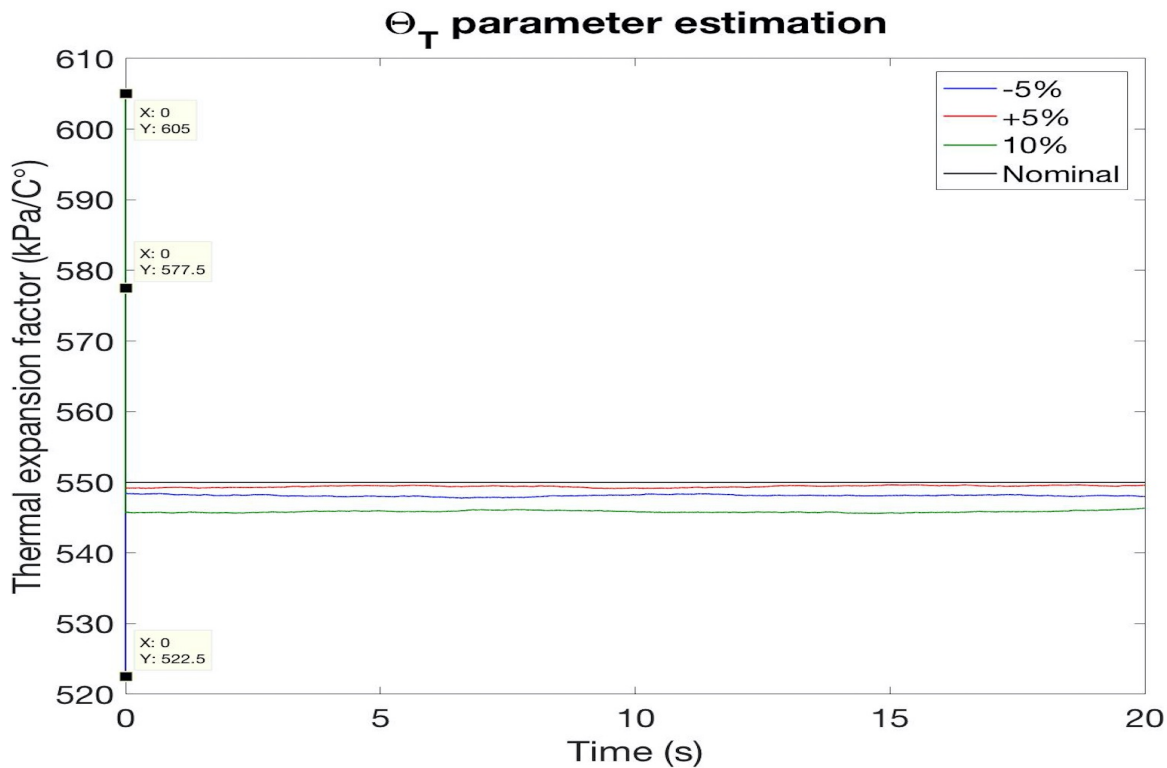


FIGURE 5.8: Thermal expansion factor UKF estimation

5.6 Tracking performance analysis in closed-loop control

In Chapter 5.6, the UKF estimation algorithm and self-sensing portion of the SMA model are combined with a PID controller to form the closed-loop control system of the SMA wire actuator as previously shown in Figure 4.4.

5.6.1 Tracking performance with State UKF

The performance of the closed-loop system is studied based on two desired displacement profiles; namely a stair-case and sinusoidal wave. In Figure 5.9, at the first stair wave, the estimated state does not follow the desired displacement profile quite well, followed by the next stair wave where the SMA wire is heated high enough to take the reverse phase transformation. From 20s to 40s, the SMA wire actuator shows a very accurate tracking ability. On the successive stair, there exists a larger tracking error as opposed to the tracking performance upon heating. This is attributed to the intrinsic low bandwidth of a shape memory alloy. From the displacement error plot, it is noticed that the error peaks correspond to the start of a change in the desired displacement. Physically speaking, these points are where the SMA actuator starts contracting back to its original position before loading.

In Figure 5.10, although initially, the maximum displacement error is larger than in Figure 5.9, the overall displacement error seems smaller over 60s. This is because there are no sudden changes in the desired displacement profile except at 30s. The tracking performance in this type of the profile remains reasonably consistent between the 1st and 2nd cycle. The large displacement error just after the peak desired displacement is again due to the limited cooling capability, taking more time to cool down to reach the Martensitic characteristic start temperature.

5. RESULTS

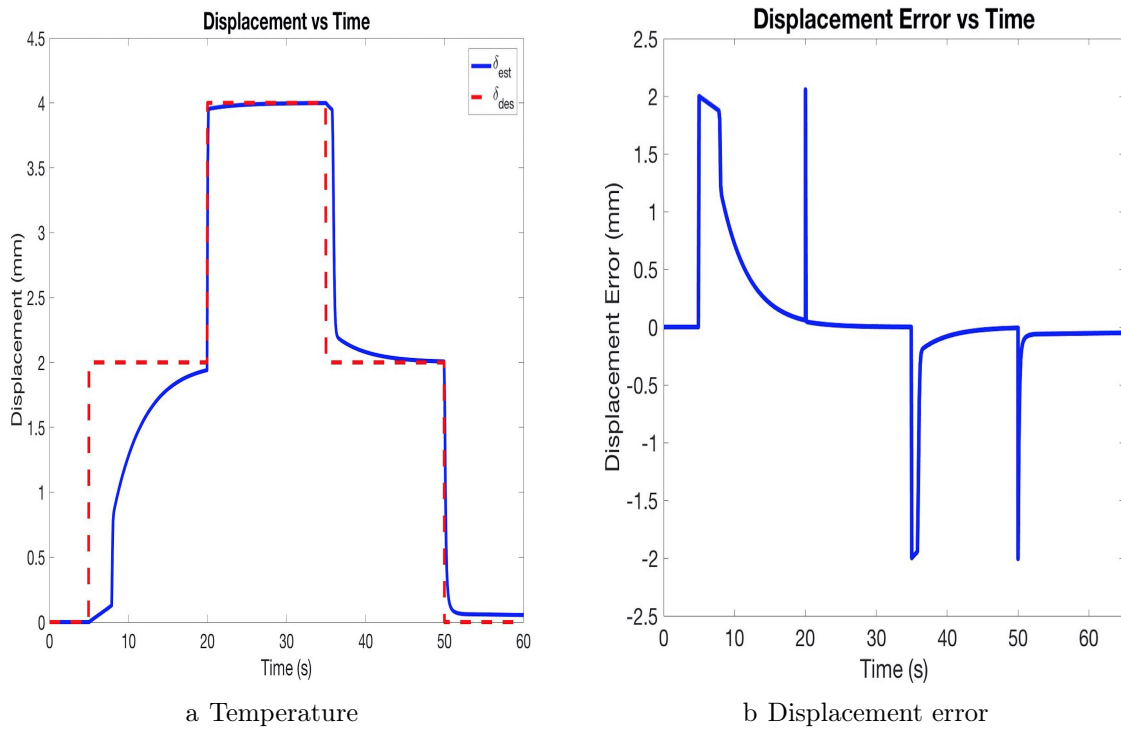


FIGURE 5.9: Displacement tracking performance in stair-case wave

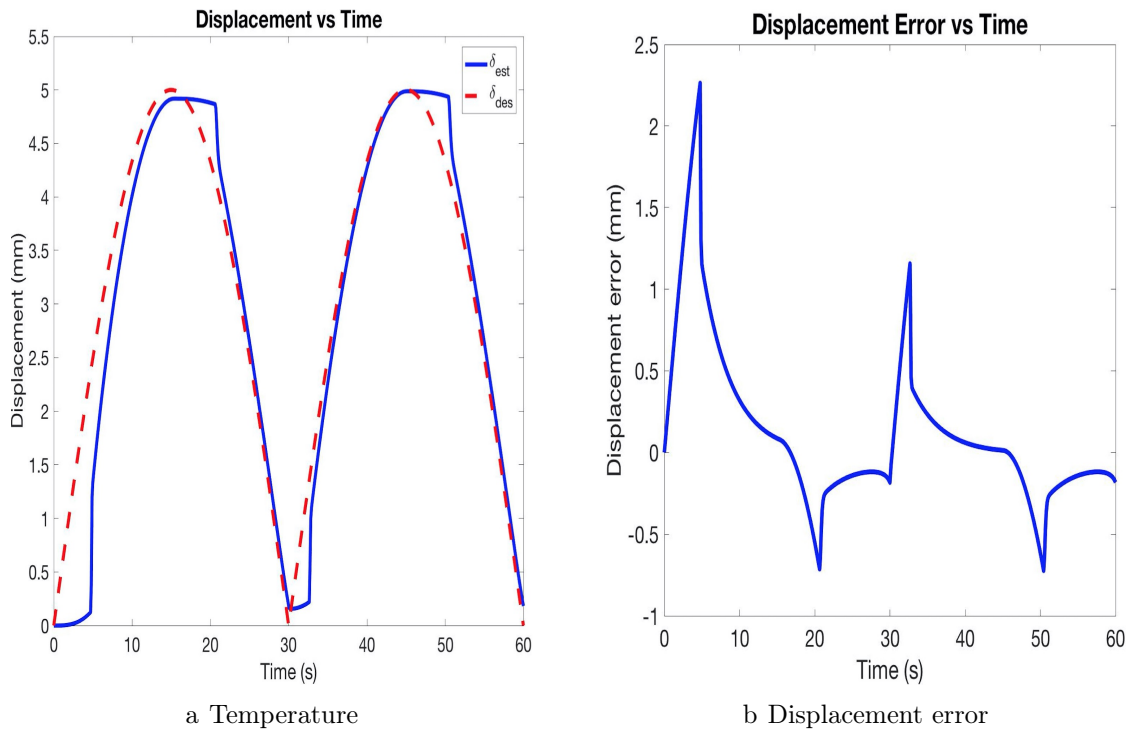


FIGURE 5.10: Displacement tracking performance in sinusoidal wave

5.6.2 Tracking performance with DUKF

For the simulation to compare between the only state UKF and DUKF in the tracking performance, the empirically derived convective heat transfer coefficient h_0 is selected as the estimated parameter from the same -10% initial condition as in Figure 5.7. In the state UKF only closed-loop control system, this parameter will not be updated, while the estimated parameter is used in the DUKF based closed-loop system. The results are as shown in Figure 5.11. In terms of the tracking accuracy of the desired displacement profile, there is no significant difference between UKF and DUKF because only 10% of one parameter changes. However, the accuracy in tracking the behavior of the nonlinear SMA actuator model is significantly different as can be seen in Figure 5.11b. The Dual Unscented Kalman Filter algorithm also captures the true behavior of the SMA actuator by estimating and updating h_0 at each iteration, while the state UKF algorithm results in more than 1mm displacement difference, which can be critical in applications where the high control accuracy is required. This is due to the transition temperature state being estimated in the UKF based on lower convective heat transfer coefficient, which results in the higher temperature estimate than the true nonlinear SMA model. A high accuracy in tracking the nonlinear SMA model is observed even at the transient stage in the DUKF algorithm, which is reasonable from the fast convergence rate of the parameter estimate as shown in Figure 5.7.

5. RESULTS

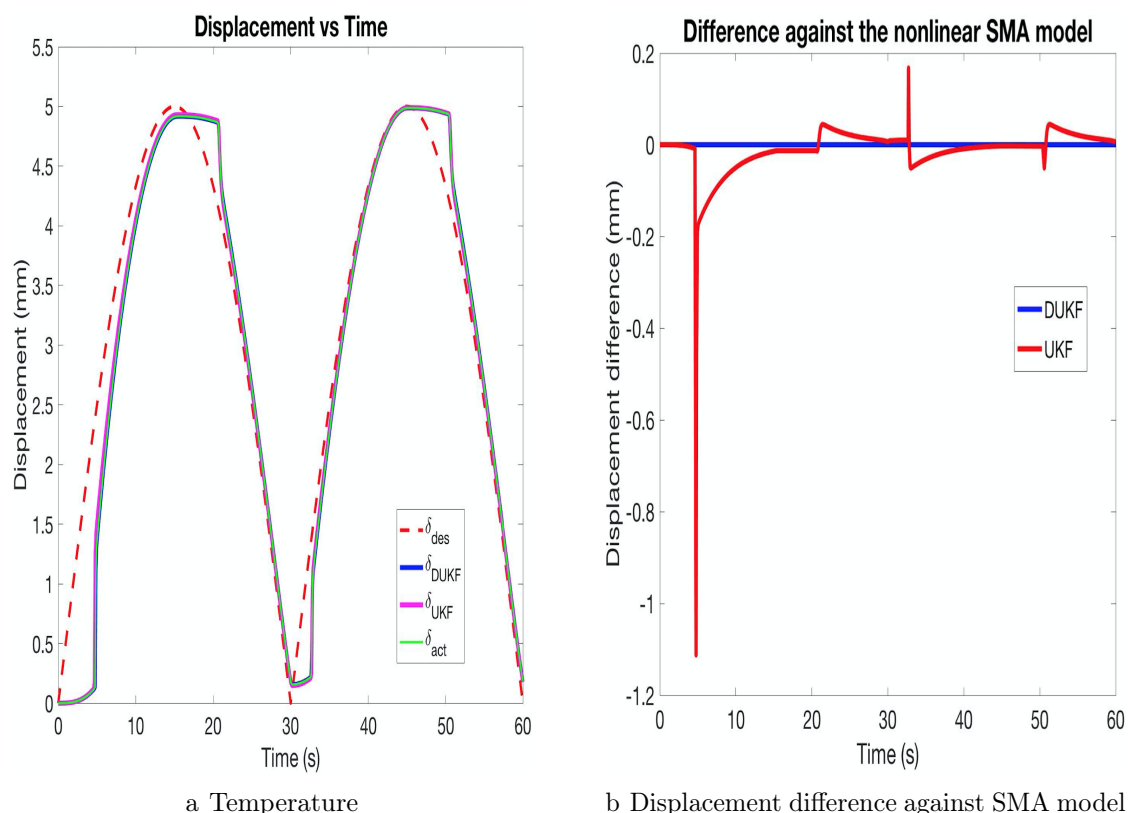


FIGURE 5.11: Comparison between UKF and DUKF

The results presented in Chapter 5 show the numerical feasibility of the Dual Unscented Kalman Filter for both state and parameter estimations in the application of the shape memory alloy wire actuator. This section provides a deeper analysis of the results and their importances in terms of the research question.

6.1 State UKF estimation

For any voltage input profiles, including more realistic simulations with additional observation noises and external disturbance, the state estimation errors or the corresponding displacement error of the SMA actuator were relatively small over the tested time range, except for the times when the shape memory alloy starts to transform its phase from one to another. These times are matched with the actuator reaching and passing through the characteristic start transformation temperatures (A_s and M_s). From Figure 5.1, the change in gradient is much higher than that observed through the experiments in Figure 2.3. This may imply that there are significant amount of modeling simplifications and assumptions, which could not be handled well in the state UKF filter. To better handle this issue, the tuning of noise covariances may be necessary. If the measurement noise covariance is large, the corresponding Kalman gain calculated will be smaller, putting less confidence on the self-sensed observation data. Adapting the measurement covariance when the phase transformation rate is

high may be a valid way to mitigate the estimation error problem.

6.2 Parameter UKF estimation

From Chapter 5.5, it was observed that the convective heat transfer coefficient was successfully estimated, converging to the nominal value used in the nonlinear SMA model, while the thermal expansion factor was converged towards the nominal value, but not to the exact value. This could be due to the fact that there may exist a strong correlation between the state variables estimated and thermal expansion factor. In the Dual Unscented Kalman Filter algorithm, the cross covariances are not explicitly estimated, meaning that $P_{xq} = P_{qx} = 0$ as it is not considered in Chapter 4.3.3. In such cases, a different UKF approach may be more suitable (e.g. joint method). However, since it still provides the acceptable accuracy in parameter estimations regardless of the correlation against the estimated state variables, the implementation of the Dual Unscented Kalman Filter algorithm into the SMA actuator system can be validated because its numerical feasibility has been proven in Chapter 5. It may be utilized in various ways, including adaptation of parameters used in the SMA models as it was conducted to mitigate uncertainties in this study and online/offline parameter identification. For the adaptation of parameters, as it was observed that the convective heat transfer coefficient reached to its nominal true value within a short amount of time (i.e. 8s), it may not be recommended to run the two filters simultaneously during the whole operational time of the SMA actuator because once the parameter is converged, the state UKF can provide a fairly accurate estimation as shown in Chapter 5 unless an estimated parameter is of strong time-varying nature. Alternatively, the DUKF based control system can be integrated with a switch mechanism similar to that used in Variable Structure Control as presented in Figure 3.3, which activates the parameter UKF filter when the displacement error exceeds a certain threshold apart from the initial cycle. In this way, the computational efficiency can be also achieved, while maintaining a reasonably accurate actuated displacement tracking with the parameter adaptation at only every few hundreds or thousands working cycles, depending on the level of accuracy required in a particular application.

6.3 Actuator tracking performance

In terms of tracking the desired reference displacement, the estimated displacement is in an acceptable agreement with the true nonlinear SMA model based on the self-sensed resistance measurements. The initial large displacement error is more attributed to the nature of a shape memory alloy; that is it does not start the reverse phase transformation unless its temperature reaches to the characteristic transformation temperature, which requires a certain level of voltage if heated via Joules heating. Figure 6.1 shows the control voltage input to the SMA actuator when tracking the stair wave displacement profile in Figure 5.9. It can be seen from the plot that the voltage gradually increases after 5s (or when the desired displacement becomes 2mm), taking up to 10s to reach the peak voltage input after which the phase transformation starts. Based on the fixed gains in the PID controller, it is not practical to have a higher voltage input at the initial stage, while considering about the overheating of a SMA wire actuator. This could be solved by implementing a nonlinear adaptive controller instead as presented in Chapter 3.2 or alternatively, integrating a fast heating mechanism proposed by Featherstone et al. [69], which can be compatible with the electrical resistance based self sensing control.

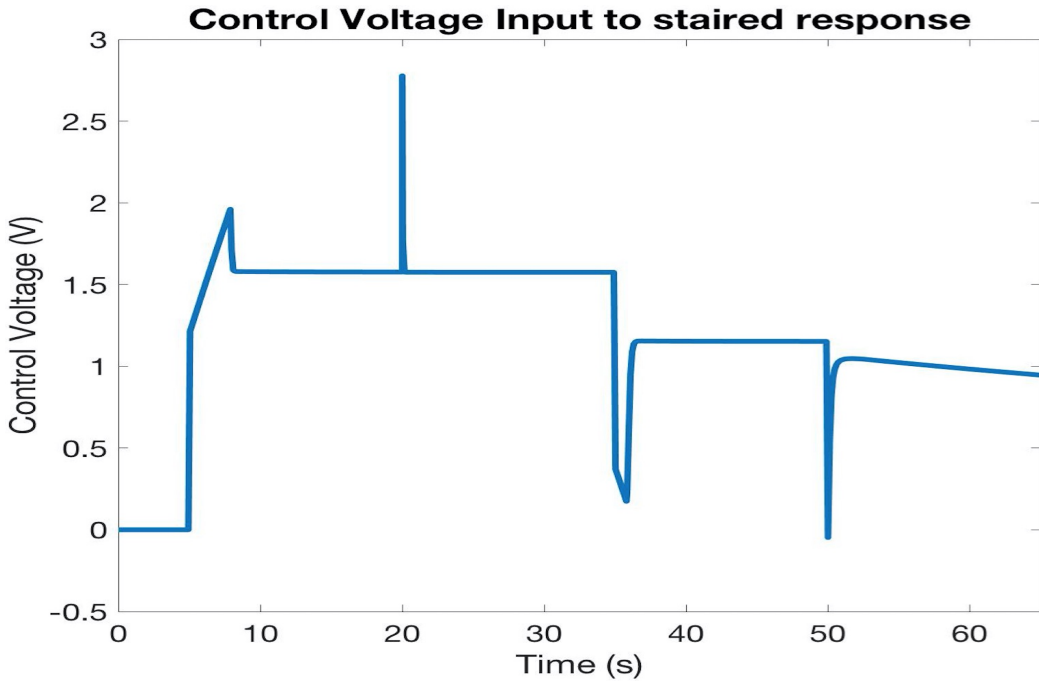


FIGURE 6.1: Control voltage input to stair wave displacement profile

In this thesis study, the numerical feasibility of a Dual Unscented Kalman Filter (DUKF) in the context of a NiTi based shape memory alloy wire actuator has been investigated and presented with a focus on approaching an uncertainty-related control issue of the SMA actuator, which has not been explored and tackled extensively in the SMA control literature.

Based on the phenomenological shape memory alloy models generally used in engineering applications, the nonlinear SMA models were developed to simulate the true behaviors of a shape memory alloy wire actuator, from which control input and electrical resistance measurement data were collected and then used in the UKF algorithms. To further reduce an uncertainty associated with measurements, while maximizing the potential of a SMA actuator as a compact-size counterpart to conventional actuators, a self-sensing approach was taken with the electrical resistance being observed to achieve the control system without any physical sensors. In the Dual Unscented Kalman Filter algorithm, the temperature and stress of a SMA wire actuator were estimated recursively to provide the estimated displacement that can be provided the SMA actuator. To control the estimated displacement in a closed-loop manner, a simple PID feedback controller was developed, which allowed the nonlinear SMA model to self-sense itself based on the input voltage, followed by the state and parameter UKF filters to provide the estimates of variable of interest.

Through the number of simulations, the performance of a UKF state filter has been proven to provide accurate estimates of the state variables, based on which it allows the accurate active control of the SMA actuator. This filter has been investigated in terms of more realistic noisy measurement data and potential external disturbances during the operational life of the SMA actuator. The parameter UKF was also studied for its performance to accurately adapt the parameters, which was found effective for some parameter, while other parameters were still observed to be in a good qualitative agreement with the expected convergence behaviors. With the DUKF configuration, it was noticed that it provided the capability of adjusting the parameters to the values used in the true nonlinear SMA model, allowing the SMA actuator to behave very similar to the actual nonlinear model. This suggests the numerical feasibility of a Dual Unscented Kalman Filter algorithm to simultaneously provide the state and parameter estimations for handling uncertainties present in a shape memory alloy actuator. The results of this study should shed a light on the importance of tackling the general control issues associated with uncertainties and encourage the SMA actuator control community to use the model-based nonlinear control algorithms with the resulting lesser associated uncertainties to achieve a better control performance of a SMA actuator. Consequently, it is believed by the author that such control and sensing techniques can promote a wider use of the shape memory alloy based actuators in various industries in future. Chapter 7.1 outlines some of the potential future works to extend this study or explore other related openings for further research in this area.

7.1 Future Work

Extending this thesis study to further can be achieved in the following points:

- Experimental verifications of the Dual Unscented Kalman Filter algorithm for both state and parameter estimations in a controlled fashion.
- Implementation of a nonlinear adaptive control algorithm in Chapter 3.2, focusing on the mitigation of initial large displacement error, while operating below the overheat temperature.

- Investigate the effects of more than one parameter estimations simultaneously with the state UKF on estimation and control performance of the SMA actuator
- Further research into the stability, robustness and disturbance rejection in the DUKF developed in this study.

Alternatively, other possible explorations related to the smart materials actuators include:

- Develop the mathematical models of a smart materials actuator through both simulation and experiments.
- Study the other smart materials based actuator and control mechanisms such as a Magnetic Shape Memory Alloy or High Temperature Shape Memory Alloy.

Bibliography

- [1] H.S. Tzou, H.-J. Lee, and S.M. Arnold. Smart materials, precision sensors/actuators, smart structures, and structronic systems. *Mechanics of Advanced Materials & Structures*, 11(4/5):367 – 393, 2004.
- [2] Micky Rakotondrabe, editor. *Smart Materials-Based Actuators at the Micro/Nano-Scale, Characterization, Control, and Applications*. Springer International Publishing AG, 2013.
- [3] Jaronie Mohd Jani, Martin Leary, Aleksandar Subic, and Mark A. Gibson. A review of shape memory alloy research, applications and opportunities. *Materials & Design (1980-2015)*, 56:1078 – 1113, 2014.
- [4] Arne Ölander. An electrochemical investigation of solid cadmium-gold alloys. *Journal of the American Chemical Society*, 54(10):3819–3833, 1932.
- [5] W. J. Buehler, J. V. Gilfrich, and R. C. Wiley. Effect of low-temperature phase changes on the mechanical properties of alloys near composition tini. *Journal of Applied Physics*, 34(5):1475–1477, 1963.
- [6] L. Sun and W. M. Huang. Nature of the multistage transformation in shape memory alloys upon heating. *Metal Science and Heat Treatment*, 51(11):573–578, 2009.
- [7] W. Huang. On the selection of shape memory alloys for actuators. *Materials & Design*, 23(1):11 – 19, 2002.
- [8] W.M. Huang, Z. Ding, C.C. Wang, J. Wei, Y. Zhao, and H. Purnawali. Shape memory materials. *Materials Today*, 13(7):54 – 61, 2010.

- [9] Shuo Wang Mohammad H. Elahinia, Ehsan Tarkesh Esfahani. *Shape Memory Alloys: Manufacture, Properties and Applications*, chapter 2: Review of the state of the art of control of SMA systems. Nova Science Publishers, Inc, 2010.
- [10] T.J. Kooman. General control framework for shape memory alloy based actuators: A phase transformation approach. Master's thesis, Faculty of Mechanical, Maritime and Materials Engineering, Delft University of Technology, June 2015.
- [11] T. A. Wenzel, K. J. Burnham, M. V. Blundell, and R. A. Williams. Dual extended kalman filter for vehicle state and parameter estimation. *Vehicle System Dynamics*, 44(2):153–171, 2006.
- [12] Mohammad H Elahinia, Mehdi Ahmadian, and Hashem Ashrafiouon. Design of a kalman filter for rotary shape memory alloy actuators. *Smart Materials and Structures*, 13(4):691, 2004.
- [13] Mohammad H. Elahinia. *Shape Memory Alloy Actuators : Design, Fabrication and Experimental Evaluation*. Wiley, 2015.
- [14] L. Sun and W. M. Huang. Nature of the multistage transformation in shape memory alloys upon heating. *Metal Science and Heat Treatment*, 51(11):573–578, 2009.
- [15] Dimitris C. Lagoudas, editor. *Shape Memory Alloys: Modeling and Engineering Applications*. Springer, 1st ed edition, 2010.
- [16] M Kök, F Dağdelen, A Aydoğdu, and Y Aydoğdu. The change of transformation temperature on niti shape memory alloy by pressure and thermal ageing. *Journal of Physics: Conference Series*, 667:012011, Jan 2016.
- [17] Mohammad H. Elahinia, Hashem Ashrafiouon, Mehdi Ahmadian, and Hanghao Tan. A temperature-based controller for a shape memory alloy actuator. *Journal of Vibration and Acoustics*, 127(3):285–291, 06 2005.
- [18] Mohammad H. Elahinia and Hashem Ashrafiouon. Nonlinear control of a shape memory alloy actuated manipulator. *Journal of Vibration and Acoustics*, 124(4):566–575, 09 2002.

-
- [19] H Funakubo, editor. *Shape Memory Alloys*, volume vol. 1 of *Precision Machinery and Robotics*. CRC Press. Gordon and Breach Science Publishers, 1987.
 - [20] Dynalloy Inc. Technical characteristics of flexinol actuator wires. Technical report, Dynalloy Inc., 2007.
 - [21] J. N. Reddy Ashwin Rao, A. R. Srinivasa. *Design of Shape Memory Alloy (SMA) Actuators*. 2015.
 - [22] D. Stoeckel, editor. *The Shape Memory Effect Å Phenomenon, Alloys and Applications*, volume pp. 1-13, Fremont, CA, 1995. Nitinol Devices and Components, Inc.
 - [23] Weimin huang. *Shape memory alloys and their application to actuators for deployable structures*. PhD thesis, Department of Engineering, University of Cambridge, march 1998.
 - [24] C. Liang and C.A. Rogers. One-dimensional thermomechanical constitutive relations for shape memory materials. *Journal of Intelligent Material Systems and Structures*, 1(2):207–234, 1990.
 - [25] L.C. Brinson. One-dimensional constitutive behavior of shape memory alloys: Thermomechanical derivation with non-constant material functions and redefined martensite internal variable. *Journal of Intelligent Material Systems and Structures*, 4(2):229–242, 1993.
 - [26] *New extension of the Kalman filter to nonlinear systems*, volume 3068, 1997.
 - [27] John B. Moore Brian D. O. Anderson. *Optimal filtering*. Prentice Hall, 1979.
 - [28] J. W. Li, X. B. Chen, and W. J. Zhang. A new approach to modeling system dynamics # x2014;in the case of a piezoelectric actuator with a host system. *IEEE/ASME Transactions on Mechatronics*, 15(3):371–380, June 2010.
 - [29] John A. Main and Ephrahim Garcia. Piezoelectric stack actuators and control system design: Strategies and pitfalls. *Journal of Guidance, Control, and Dynamics*, 20(3):479–485, 2017/06/06 1997.
 - [30] W. Huang. On the selection of shape memory alloys for actuators. *Materials & Design*, 23(1):11 – 19, 2002.

- [31] W.M. Huang, Z. Ding, C.C. Wang, J. Wei, Y. Zhao, and H. Purnawali. Shape memory materials. *Materials Today*, 13(7):54 – 61, 2010.
- [32] Ziqiang Chi and Qingsong Xu. Recent advances in the control of piezoelectric actuators. *International Journal of Advanced Robotic Systems*, 11(11):182, 2014.
- [33] Keekyoung Kim, Xinyu Liu, Yong Zhang, and Yu Sun. Micronewton force-controlled manipulation of biomaterials using a monolithic mems microgripper with two-axis force feedback. In *2008 IEEE International Conference on Robotics and Automation*, pages 3100–3105, May 2008.
- [34] Neal B. Hubbard, Martin L. Culpepper, and Larry L. Howell. Actuators for micropositioners and nanopositioners. *Applied Mechanics Reviews*, 59(6):324–334, 11 2006.
- [35] T.G. King, M.E. Preston, B.J.M. Murphy, and D.S. Cannell. Piezoelectric ceramic actuators: A review of machinery applications. *Precision Engineering*, 12(3):131 – 136, 1990.
- [36] Q. Xu and Y. Li. Sliding mode control of a piezo-driven micropositioning system using extended kalman filter. In *2010 IEEE International Conference on Automation and Logistics*, pages 427–432, Aug 2010.
- [37] Delijic K. Asanovic, V. The mechanical behavior and shape memory recovery of cu-zn-al alloys. *Metalurgijad- J Metall*, 2007.
- [38] W. Khalil, L. Saint-Sulpice, S. Arbab Chirani, C. Bouby, A. Mikolajczak, and T. Ben Zineb. Experimental analysis of fe-based shape memory alloy behavior under thermomechanical cyclic loading. *Mechanics of Materials*, 63:1 – 11, 2013.
- [39] Stanciu S Cimpoesu R Constantin B Paraschiv C et al. Cimpoesu N, Dragos Ursanu A. Preliminary results of copper based shape memory alloys analyze used for mems applications. *Appl Mech Mater*, 2013.
- [40] Concilio. Antonio ecce. Leonardo, editor. *Shape Memory Alloy Engineering: For Aerospace, Structural and Biomedical Applications*. Elsevier Science, September 2014.

-
- [41] A Sato, E Chishima, K Soma, and T Mori. Shape memory effect in gamma to/from epsilon transformation in fe-30mn-1si alloy single crystals. *Acta Metallurgica*, 30(6):1177 – 1183, 1982.
 - [42] S. Majima, K. Kodama, and T. Hasegawa. Modeling of shape memory alloy actuator and tracking control system with the model. *IEEE Transactions on Control Systems Technology*, 9(1):54–59, Jan 2001.
 - [43] E. Shameli, A. Alasty, and H. Salaarieh. Stability analysis and nonlinear control of a miniature shape memory alloy actuator for precise applications. *Mechatronics*, 15(4):471 – 486, 2005.
 - [44] N Ma and G Song. Control of shape memory alloy actuator using pulse width modulation. *Smart Materials and Structures*, 12(5):712, 2003.
 - [45] M. Sreekumar, M. Singaperumal, T. Nagarajan, M. Zoppi, and R. Molfino. Recent advances in nonlinear control technologies for shape memory alloy actuators. *Journal of Zhejiang University-SCIENCE A*, 8(5):818–829, 2007.
 - [46] V. Utkin. Variable structure systems with sliding modes. *IEEE Transactions on Automatic Control*, 22(2):212–222, Apr 1977.
 - [47] Seung-Bok Choi. Position control of a single-link mechanism activated by shape memory alloy springs: experimental results. *Smart Materials and Structures*, 15(1):51, 2006.
 - [48] Soo-Cheol Lim, Jong-Sung Park, Seung-Bok Choi, and Young-Pil Park. Non-contact start/stop motion control of hdd suspension using shape memory alloy actuators. *Smart Materials and Structures*, 10(5):1069, 2001.
 - [49] Mohammad H. Elahinia, T. Michael Seigler, Donald J. Leo, and Mehdi Ahmadian. Nonlinear stress-based control of a rotary sma-actuated manipulator. *Journal of Intelligent Material Systems and Structures*, 15(6):495–508, 2004.
 - [50] D. Grant and V. Hayward. Variable structure control of shape memory alloy actuators. *IEEE Control Systems*, 17(3):80–88, Jun 1997.
 - [51] A.M. Annaswamy K.S. Narendra. *Stable Adaptive Systems*. Dover Publications, 2004.

- [52] G. Song, V. Chaudhry, and C. Batur. A neural network inverse model for a shape memory alloy wire actuator. *Journal of Intelligent Material Systems and Structures*, 14(6):371–377, 2003.
- [53] N. B. Kha and K. K. Ahn. Position control of shape memory alloy actuators by using self tuning fuzzy pid controller. In *2006 1ST IEEE Conference on Industrial Electronics and Applications*, pages 1–5, May 2006.
- [54] N. T. Tai and K. K. Ahn. Output feedback direct adaptive controller for a sma actuator with a kalman filter. *IEEE Transactions on Control Systems Technology*, 20(4):1081–1091, July 2012.
- [55] Mohammad H Elahinia and Mehdi Ahmadian. Application of the extended kalman filter to control of a shape memory alloy arm. *Smart Materials and Structures*, 15(5):1370, 2006.
- [56] H. Gurung and A. Banerjee. Self-sensing shape memory alloy wire actuator based on unscented kalman filter. *Sensors and Actuators A: Physical*, 251:258 – 265, 2016.
- [57] H Gurung and A Banerjee. Development of an extended kalman filter for the self-sensing application of a spring-biased shape memory alloy wire actuator. *Smart Materials and Structures*, 25(2):025012, 2016.
- [58] Pavaneesh Narayanan. Sensor-less control of shape memory alloy using artificial neural network and variable structure controller. Master’s thesis, University of Toledo, 2014.
- [59] K. Ikuta, M. Tsukamoto, and S. Hirose. Shape memory alloy servo actuator system with electric resistance feedback and application for active endoscope. In *Proceedings. 1988 IEEE International Conference on Robotics and Automation*, pages 427–430 vol.1, Apr 1988.
- [60] Ranjan Mukherjee, Thomas F. Christian, and Richard A. Thiel. An actuation system for the control of multiple shape memory alloy actuators. *Sensors and Actuators A: Physical*, 55(2):185 – 192, 1996.
- [61] M Pozzi and G Airoldi. The electrical transport properties of shape memory alloys. *Materials Science and Engineering: A*, 273:300 – 304, 1999.

-
- [62] X. D. Wu, Y. Z. Fan, and J. S. Wu. A study on the variations of the electrical resistance for niti shape memory alloy wires during the thermo-mechanical loading. *Materials & Design*, 21(6):511–515, 12 2000.
 - [63] L.C. Brinson. One-dimensional constitutive behavior of shape memory alloys: Thermomechanical derivation with non-constant material functions and redefined martensite internal variable. *Journal of Intelligent Material Systems and Structures*, 4(2):229–242, 1993.
 - [64] A. Banerjee, B. Bhattacharya, and A. K. Mallik. Forward and inverse analyses of an sma actuated compliant link. *Journal of Mechanisms and Robotics*, 3(2):021003–021003–10, 03 2011.
 - [65] Timothy Charles Brunette. A novel shape memory alloy actuator for solar sailing attitude control. Master’s thesis, Department of Aerospace, Mechanical and Mechatronic Engineering, October 2016.
 - [66] Eric Wan and Rudolph Van Der Merwe. Chapter 7 the unscented kalman filter. In *Kalman Filtering and Neural Networks*, pages 221–280. Wiley, 2001.
 - [67] Anxi Yu, Ye Liu, Jubo Zhu, and Zhen Dong. An improved dual unscented kalman filter for state and parameter estimation. *Asian Journal of Control*, 18(4):1427 – 1440, 2016.
 - [68] Matthew C. Vandyke, Jana L. Schwartz, and Christopher D. Hall. Unscented kalman filtering for spacecraft attitude state and parameter estimation. In *in Proceedings of the AAS/AIAA Space Flight Mechanics Conference, no. AAS 04-115, (Maui*, 2004.
 - [69] Roy Featherstone and Yee Harn Teh. *Improving the Speed of Shape Memory Alloy Actuators by Faster Electrical Heating*, pages 67–76. Springer Berlin Heidelberg, Berlin, Heidelberg, 2006.